Advancing Last Glacial Maximum paleoclimate reconstructions in Europe using pollen data: a multi-method (mega)biomization approach

Fénisse G.[1*], Chevalier M.[2], Peyron O.[3], Bekaert D.V.[1], Blard P.-H.[1,4]

1. *Centre de Recherches Pétrographiques et Géochimiques UMR 7358, 15 Rue Notre Dame des Pauvres, 54 500 Vandoeuvre-lès Nancy, France*
2. *Institute of Geosciences, Sect. Meteorology, Rheinische Friedrich-Wilhelms-Universität Bonn, Auf dem Hügel, 20, 53 121 Bonn, Germany*
3. *Institut des Sciences de l'Evolution-Montpellier (ISEM), University of Montpellier, UMR 5554 CNRS, EPHE, IRD, Montpellier, France*
4. *Laboratoire de Glaciologie, Département de Géosciences, Environnement et Société, ULB, Brussels, Belgium*

Journal: Climate of the past (CP)

*Corresponding author.
E-mail address: gabriel.fenisse@univ-lorraine.fr (G.Fénisse).

Abstract

Pollen records are one of the most spatially and temporally resolved proxies for reconstructing past vegetation dynamics, environmental changes and climate variability. Over the past decade, a large variety of methods based on different ecological or mathematical concepts has been used to reconstruct paleoclimatic conditions from pollen assemblages. However, the accuracy of these climate reconstructions strongly depends on the choice of the modern calibration dataset, the taxonomic resolution, and/or the modelling assumptions. The lack of a univocal response still limits the application of pollen-based climate reconstructions to assess key climate changes over multiple time periods especially during the Last Glacial Maximum (LGM, ~23-19 kyr BP). Here, we present a multi-method approach, including the Modern Analogue Technique (MAT), the Weighted Averaging Partial Least Squares regression (WA-PLS) and the probability density function-based Climate REconstruction SofTware (CREST), to reconstruct European climates during the LGM. The quality and performance of our climate reconstructions show strong heterogeneity when based on large calibration datasets encompassing wide climatic and vegetation gradients, making local sampling for climate reconstructions difficult. Instead of sampling the global calibration dataset, we test the effect of the latest biomization and megabiomization methods (local calibrations based on megabiome procedures) on climate reconstructions by introducing a new biome-based approach. Unlike previous studies, we use the weighted mean of climate variables from all megabiome scores rather than only considering the dominant (i.e., highest score) megabiome. This significantly reduces some of the statistical noise of climate reconstructions, drastically minimizing threshold and non-linear effects associated with megabiome classification changes. With these methodological advancements and our multi-method comparison, we evaluate the uncertainties (RMSEP) of the paleoclimate reconstructions for the LGM in Europe. Across climate reconstruction methods (MAT, WA-PLS and CREST methods), European LGM annual temperatures from the biomization method were on average 6.7$\pm$2.2°C (mean SD) colder than today, consistent with megabiomization results (7.4$\pm$2.3 °C colder). Winter temperature (mean temperature of the coldest month, MTCO) results exhibit substantial spatial variability across Europe. Local calibration techniques significantly reduce uncertainties in LGM MTCO reconstructions, but they remain highly sensitive to the choice of calibration datasets.

I. Introduction

Reconstructing past climates is essential for understanding the mechanisms driving glacial–interglacial variability and for evaluating the reliability of climate model simulations. Pollen assemblages preserved in marine, lacustrine and peat bog sediments constitute robust proxies for reconstructing past climatic conditions (e.g., *Chevalier et al., 2020*). Pollen-based paleoclimate reconstructions are available for many regions (e.g., Europe, Eurasia, Mediterranean areas) and for various time-periods as the Eemian (e.g., *Brewer et al., 2008; Sinopoli et al., 2018*), the Holocene (e.g., *Davis et al., 2003; Peyron et al., 2013; Salonen et al., 2019; Herzschuh et al., 2022a*) and other past key periods (e.g., *Charton et al., 2025; Zumaque et al., 2025*). While reconstructions of warm interglacial periods such as the Eemian and the Holocene generally show good agreement across different methods (*Sinopoli et al., 2018; Sassoon et al., 2025*), this consistency tends to break down for glacial periods (*Guiot et al., 1990; Brewer et al., 2008; Charton et al., 2025*). In particular, accurately reconstructing temperature and precipitation during the Last Glacial Maximum (LGM, ~19–23 thousand years ago; *Hughes et al., 2013*) remains a persistent challenge as environmental gradients are strong and vegetation-climate relationships are complex (*Peyron et al., 1998; Bartlein et al., 2011; Davis et al., 2024*). Over the past decades, a wide range of approaches has been developed from pollen data to address the issue of glacial climate reconstructions. These include the Modern Analogue Technique (MAT, *Guiot et al., 1990*), transfer functions via the Weighted Averaging Partial Least Squares regression (WA-PLS, *Ter Braak and Juggins, 1993*), the Plant Functional Type method (PFTs, *Peyron et al., 1998*) and the Inverse Modelling approach (*Guiot et al., 2000; Wu et al., 2007*). The Inverse modelling and the algorithms developed by *Prentice et al, (2022)* and *Cleator et al, (2020)* take into account the CO_2 effect in the climate reconstructions: the algorithms explicitly account for the physiological effects of low atmospheric CO_2 concentrations ($pCO_2 \approx 180$ ppm) on LGM vegetation. Despite these methodological advances, substantial discrepancies remain between the results derived from these reconstruction methods and those simulated by climate models (e.g., *Jost et al., 2005; Cleator et al., 2020*). Such inconsistencies highlight the complexity of reconstructing reliable glacial climates, particularly for regions such as Europe and the Mediterranean Basin (*Zumaque et al., 2025; Charton et al., 2025*). Improving the robustness and comparability of paleoclimate reconstructions for cold periods thus remains a key objective for the paleoclimate community.

Recent studies have emphasized that the choice of reconstruction method can significantly influence reconstructed climatic parameters (*Dugerdil et al., 2021, 2025; Robles et al., 2023; Charton et al., 2025*) as the methods and assumptions used are based on different ecological and mathematical/statistical concepts and algorithms (see *Chevalier et al., 2020* for a review). They assume that proxy-climate relationships remain constant over time and that pollen variations primarily reflect climate variations. Among all the methods available to reconstruct past climate changes from pollen data, the MAT and the WA-PLS are the most commonly used in paleoclimatology (e.g. *Davis et al., 2003, 2024; Birks et al., 2004; Mauri et* *al., 2014, 2015; Liu et al., 2020; Herzschuh et al., 2022a*). Most studies have applied these approaches individually, with only a few combining MAT and WA-PLS (*Sinopoli et al., 2021; Herzschuh et al., 2022a; Geng et al., 2025*). These studies demonstrated that reconstruction results can vary substantially between methods, mainly due to variations in modern pollen–climate calibration datasets, spatial coverage and the ecological tolerances assigned to plant taxa. They also highlighted the influence of fossil record quality and the reliability of the quantitative reconstruction methods themselves (e.g., *Brewer et al., 2008; Peyron et al., 2013; Chevalier et al., 2020; Dugerdil et al., 2021, 2025*).

To enhance the reliability of paleoclimatic reconstructions, a methodological framework combining several complementary approaches has been developed over the last decade (*Peyron et al., 2005, 2011; 2013, Brewer et al., 2008; Salonen et al., 2019*). This multi-method approach highlights that significant discrepancies can arise depending on the reconstruction method applied. The reliability of each method is influenced by the composition of the pollen assemblages, meaning that the most appropriate or robust approach may differ depending on the taxa present and the specific period being studied. These studies have nevertheless introduced important methodological advances, representing a significant improvement over single-method approaches, even though assessing the robustness of the results remains a complex task. The most robust method can be identified and validated by comparing its results with independent proxy evidence obtained from the same sediment core, such as chironomid assemblages or molecular biomarkers (*d'Oliveira et al., 2023; Robles et al., 2023; Martin et al., 2020*). The multi-method approach includes various methods as MAT, WA-PLS, and machine-learning techniques (e.g., Random Forest, Boosted Regression trees) (e.g., *Salonen et al., 2012, 2019; Dugerdil et al., 2021; Robles et al., 2022, 2023; d'Oliveira et al., 2023, 2025, Sassoon et al., 2025; Charton et al., 2025*). Applying this multi-method approach to the quantification of climatic conditions during glacial periods appears highly promising, yet such applications remain exceptionally scarce (e.g., *Brewer et al., 2008; Charton et al., 2025*).

Statistical methods such as MAT and WA-PLS are based on fixed distance-based vegetation samples and linear relationships between pollen taxa and climate variables, respectively. These relationships may oversimplify ecological responses and fail to account for uncertainties in both modern calibration datasets and fossil assemblages. One promising avenue to better quantify climatic parameters from pollen data during the LGM is probabilistic approaches like the Probability Density Functions (PDFs) method (*Kühl et al., 2002, 2010; Trasune et al., 2024; Seirienné and Kisielienė, 2014*). Probabilistic approaches (e.g., *Kühl et al., 2002; Kühl and Litt, 2003; Gebhardt et al., 2008*) explicitly model these uncertainties and integrate the full probability distributions of taxa–climate relationships, thereby capturing the complete range of climate tolerances of the observed taxa. One version of the PDF-method named CREST (Climate REconstruction SofTware, *Chevalier et al., 2014, Chevalier, 2022*) describes the conditional responses of taxa assemblages to climate variables, by combining generally unimodal distributions of reconstructed climate spaces from each taxon. The main innovations of CREST are (i) accounting for taxonomic uncertainties in pollen data, and (ii) using presence-only data rather than presence/absence data. The multiplication of these PDFs yields a likelihood distribution, which represents the full range of climatic conditions in which a given assemblage can occur, derived from the statistical analysis of modern presence-only data (*Chevalier, 2022*).

Another promising opportunity to further enhance the reliability of climate reconstructions for glacial periods is to integrate biomization techniques within each reconstruction method following *Prentice et al., (1996)*. Applying such biome-based constraints has been tested with the MAT method and appears to be a particularly promising (*Guiot et al., 1993*) yet still underexplored approach (*Dugerdil et al., 2025*). Biomization techniques have been developed to convert modern and fossil pollen assemblages into specific vegetation types (i.e., biomes or megabiomes), thereby linking the ecological, physiological and physiognomic data with both current and past climatic and environmental conditions (*Prentice et al., 1996; Li et al., 2024, Dugerdil et al., 2025*). These techniques have been widely employed to reconstruct past regional vegetation patterns particularly since the LGM (e.g., *Peyron et al., 1998; Dallmeyer et al., 2019, biome 6000 project and references therein*; *Li et al., 2024*). While such approaches can arguably improve climate interpretations and facilitate comparisons across spatial and temporal scales, most studies have used them as a way to drastically restrict the ranges of paleoclimate reconstructions by relying only on the dominant biome (i.e., the biome with the highest score) (e.g., *Guiot et al., 1993; Tarasov et al., 1999, 2013; Davis et al., 2003, 2024*). However, transitional states, ecological gradients, and the variability of biome scores are often overlooked in these studies, potentially amplifying threshold effects and non-linearities in the reconstructions (*Dallmeyer et al., 2019*). A crucial step toward improving the accuracy of paleoclimate reconstructions is therefore to better use biome information to inform the modern calibration dataset underpinning the different reconstruction methods.

Across Europe, LGM pollen records generally reveal a high diversity of forests, steppes, and tundra (*Peyron et al., 1998; Davis et al., 2024*), although cold steppe environments were predominant (e.g., *Binney et al., 2017; Davis et al., 2024*), pointing towards more arid climatic conditions than today. However, because modern cold climates are underrepresented in Europe, climate reconstructions remain challenging. Although Europe exhibits an exceptional diversity of continental proxy records, the magnitude and spatial patterns of LGM cooling are still widely debated. This uncertainty largely arises because different proxies often yield divergent reconstructions of temperature change (e.g., *Davis et al., 2024*), and substantial disagreements persist between climate model simulations and proxy-based reconstructions (e.g., *Bartlein et al., 2011; Cleator et al., 2020; Kageyama et al., 2021*). Seasonality during the LGM is primarily documented by pollen data (*Davis et al., 2024*) but remains poorly constrained, despite its potentially uncertain impact on reconstructed LGM cooling signals. Quantifying European paleoclimates is also particularly important for better constraining the role of continental thermal amplification in climate dynamics (*Seltzer et al., 2021*) and for evaluating future climate changes using climate models (*Ramstein et al., 2007; Harrison et al.,* *2014*) within the framework of the Paleoclimate Modelling Intercomparison Projects (PMIP; *Joussaume et al., 1999; Braconnot et al., 2012*). Although many climate reconstructions have been carried out for the LGM in Europe (*Peyron et al., 1998; Jost et al., 2005; Wu et al., 2007, Guiot et al., 2000, Davis et al., 2024*), they generally rely on a single reconstruction method and are based on different datasets, which can contribute to inconsistencies among the results.

In this study, we present a unique methodological framework that combines MAT, WA-PLS, and CREST to provide robust climate estimates for Europe during the LGM. Our goal is to significantly improve the accuracy of paleoclimate reconstructions by adapting biomization techniques - both the classical biomization (*Prentice et al., 1996*) and the megabiomization (*Li et al., 2024*) - to our pollen datasets. We use biomization as a constraint to select the most suitable modern pollen samples, thereby enhancing the calibration step within each reconstruction method. Using these approaches, we generate specific calibration datasets that are restricted to single biomes. We also use biomization scores that consider not only dominant biomes to achieve more robust climate reconstructions but also reconstructions based on all biome information to account for biomization uncertainties. We test our multi-method framework on two glacial time periods: (i) to reconstruct climate changes during the LGM using the well-known pollen record from Lake Bouchet (France), and (ii) to reconstruct spatial climate patterns across Europe and the Mediterranean region during the LGM.

II. Methods

II.1 - Climate reconstruction methods

We apply three distinct approaches, grounded in different ecological and modelling assumptions, to the same modern and fossil datasets, to identify and discuss the methodological biases specific to each reconstruction method.

II.1.1 - Assemblages approach: Modern Analogue Technique (MAT)

The Modern Analogue Technique (MAT; *Overpeck et al., 1985; Guiot, 1990*) is widely used to reconstruct past climate variations over time scales ranging from the last million years to the Holocene, and has been applied in particular to glacial periods (*Guiot et al., 1993; Davis et al., 2024; Zumaque et al., 2025; Charton et al., 2025*). It measures the dissimilarity between a fossil pollen assemblage and a set of modern assemblages from the modern dataset (*Guiot et al., 1989, 1990*). Climate reconstructions are performed by estimating a dissimilarity coefficient (hereafter SQChord, for “Squared chord distance”, (*Overpeck et al., 1985*) based on the closest modern analogues, using an optimal number of analogues “k” that minimizes the RMSEP (i.e., Root Mean Squared Error of Prediction, *Juggins, 2020*). This parameter “k” is specific to each climatic variable and fossil sequence (“k” from 8 to 10). Generally speaking, the MAT method appears to perform better with pollen taxa that are diverse and poorly resolved taxonomically like family (*Birks et al., 1005, Willimas and Shuman, 2008, Viau and*

Gajewski, 2009). We used the *rioja* package in R (Analysis of Quaternary Science data, version 1.0-6, R Core Team, https://cran.r-project.org/web/packages/rioja/index.html; *Juggins, 2020*) to perform MAT reconstructions. Climate reconstruction uncertainties were quantified using the root mean square error of prediction (RMSEP) derived from leave-one-out cross-validation.

II.1.2 - Transfer function: Weighted Partial Least Squares method (WA-PLS)

The Weighted Averaging Partial Least Squares method (WA-PLS; *Ter Braak and Juggins, 1993*) is a transfer function based on climatic optima and tolerances of a pollen taxon defined by its spatial niches. With this method, the climatic responses of taxa are assumed to be Gaussian (*Ter Braak and Looman, 1986*). This reconstruction method assumes unimodal (Gaussian) species response. The number of components (i.e., portion of the covariance between species abundance data and environmental variables) for paleoclimate reconstructions was selected based on those that produce the lowest root mean square error (RMSEP), a high prediction linear correlation coefficient (R^2), and less biased reconstructions to minimize mean and maximum bias (*Ter Braak and Juggins, 1993*). A minimization of the number of components (npls; *Ter Braak and Juggins, 1993*) is performed to weight and integrate potential interactions between taxa, in addition to the link that connects them to the climate. The *rioja* package was also used to carry out WA-PLS reconstructions. Uncertainties for WA-PLS reconstructions were similarly assessed through RMSEP obtained via leave-one-out cross-validation.

II.1.3 - Probability Density approach: Climate REconstruction SofTware (CREST)

Probabilistic methods provide more accurate and flexible climate reconstructions than statistical methods, with lower dependence on taxonomic resolution (*Netzel et al., 2025*). CREST describes the conditional responses of taxa assemblages to climate variables by integrating modern pollen–climate relationships (*Chevalier et al., 2014; Chevalier, 2022*). Most often, when pollen is identified at the genus or family level, the probabilistic method combines the individual species' parametric PDFs into a single PDF representing the pollen observed in the fossil sequence. Once estimated for all taxa, the PDFs for the taxa present in a sample are multiplied together, each weighted according to its observed abundance. CREST is particularly well suited for regions where pollen data are scarce or geographically unevenly distributed (*Chevalier, 2019; Chevalier et al., 2020*). In detail, this method defines the conditional response of a plant species to a climate as a parametric PDF. The taxon-climate link is established by combining these PDFs, weighted by the abundance species that make up the genera and families of the observed pollen. A composite likelihood distribution is obtained by multiplying the individual PDFs, providing a complete probabilistic representation of the climatic conditions compatible with the observed assemblage - thus accounting for the full ecological range rather than only optimal conditions. This approach allows CREST to quantify uncertainty explicitly, offering a robust framework for evaluating reconstruction reliability and comparing it with other statistical methods (MAT or WA-PLS).

To date, CREST has proven particularly effective in regions with sparse or poorly sampled data where other techniques cannot readily be used (*Chevalier et al., 2020*) and has been widely applied to several tropical ecosystems such as savannas (e.g., *Chevalier and Chase, 2015, 2016; Chevalier et al., 2021*). CREST reconstructions were generated using the *CrestR* package (https://github.com/mchevalier2/crestr, *Chevalier, 2022*).

III. Pollen Datasets

III.1 - Fossil pollen dataset

43 European fossil pollen samples spanning the LGM 19-23 kyr (cal BP) were selected (**Table 1**). Locations of pollen records, data sources, archive types, identification number, taxonomic diversity and resolution of pollen data are summarized in **Table 1**. Most fossil pollen data used in this study have been recently compiled by *Davis et al. (2024)*. Additional European fossil records that were not included in *Davis et al. (2024)* are reported in **Table 1** and in **Appendix 1**. Aquatic and anthropic pollen taxa were excluded from the LGM fossil pollen assemblages. Pollen assemblages were extracted from databases, such as ACER 1.0 (*Sanchez Goñi et al., 2017*), PANGAEA Database (https://www.pangaea.de/), and Neotoma Paleoecology Database (https://www.neotomadb.org/ ; *Williams et al., 2018*). Raw pollen counts were used when available or digitized from the published diagrams (**Table 1**). Lakes are the most abundant archive, and peat bogs are second, followed by alluvial and colluvial sediments (**Fig Appendix 1.a**). One site sequence (Venice) contains only 7 taxa, while others include up to 70 taxa, with 80% of sequences having more than 10 taxa, reflecting differences in taxonomic resolution and geographical location (**Fig Appendix 1.b**). While CREST remains effective with a small number of taxa (~8–10; *Chevalier, 2019*) due to the use of continuous probability distributions, MAT and WA-PLS generally require ≥10 taxa to produce reliable climate reconstructions (*Guiot et al., 1993; Peyron et al., 1998*).

Shrub and non-arboreal taxa dominate the LGM pollen assemblages (from 40 to 80%), except for certain records like Azzano Decimo, Rio Diodis and Pian del Lago, Orgiano records (northern Italy) for which we observe a prevalence of Pinus (>40%; **Fig appendix 1.c**). A table summarizing each taxon and vegetation types is available in **Appendix 1**. Most of the LGM samples are dominated by arid-adapted taxa (including Poaceae, Artemisia and Chenopodiaceae/Amaranthaceae). Steppic taxa such as Poaceae and *Artemisia* primarily dominate lower-latitude areas (<40°N), although, the high pollen productivity and wind transport of *Artemisia* taxa could somehow overestimate the abundance of steppic biomes (*Xu et al., 2010*).

In contrast to the study of *Davis et al. (2024)*, marine pollen records were excluded here due to taxonomic, preservation, and chronological biases when compared to terrestrial records (*Daniau et al., 2019; Xu et al., 2016*). However, the “Les Echets” record was excluded because of incomplete dating information, such as uncalibrated radiocarbon years and/or dating uncertainties.

The Lake du Bouchet pollen sequence (Eastern France) serves as a reference to study potential methodological biases in reconstructing LGM climates. Its high temporal resolution, continuity, and taxonomic richness (56 pollen taxa) make it particularly valuable for assessing the impact of different reconstruction techniques.

From all pollen data, a harmonization table was extracted from *LegacyPollen 2.0* (*Li et al., 2024; Herzschuh et al., 2022b*) and processed to match the identification of pollen data between modern and fossil samples.

SiteName	***Latitude (°N)***	***Longitude (°E)***	***Elevation (m)***	***TANN Modern (°C)***	***PANN Modern (mm)***	***MTCO Modern (°C)***	***MTWA Modern (°C)***	***Archive***	***Country***	***Source***	***Reference***	***Data Type***	***Biomes (best) 19-23 kyrs***	***Megabiomes (best) 19-23 kyrs***
Lake Xinias (1)	39.05	22.27	500	15.0	690.6	3.0	23.6	Lake	Greece	EPD (E#976)	Bottema (1979)	Raw Count	**COST**	**STEP**
Cova de les Malladetes (2)	39.06	-0.32	20	17.4	542.2	9.2	23.1	Cave	Spain	Publi.	Dupré Ollivier. (1988)	Digitised	**TUND**	**TEFO**
Navarrés (3)	39.10	0.68	225	16.7	546.9	7.3	24.8	Peat Bog	Spain	EPD (E#469)	Carrión & Dupré-Olivier. (1996)	Raw Count	**COST**	**TEFO**
Megali Limni (4)	39.10	26.30	323	15.6	724.1	8.6	25.4	Lake	Greece	Publi.	Margari et al.. (2009)	Digitised	**COST**	**TEFO**
Ioannina (5)	39.75	20.85	470	14.2	1100.1	1.1	21.5	Peat Bog	Greece	ACER	Tzedakis et al.. (2004)	Raw Count	**COST**	**TEFO**
Lake Iznik (6)	40.43	29.53	88	13.4	713.0	3.7	23.0	Lake	Turkey	EPD (E#714)	Miebach et al.. (2016)	Raw Count	**COST**	**TEFO**
Lago Grande di Monticchio (7)	40.94	15.60	1326	11.2	686.9	3.8	24.3	Lake	Italy	EPD (E#932)	Watts et al.. (1996)	Raw Count	**COST**	**TEFO**
Mire Straldzha Kupena-3 (8)	40.98	24.31	1356	10.1	893.8	4.4	25.0	Lake	Bulgaria	EPD (E#209)	Tonkov et al.. (2014)	Digitised	**COST**	**TEFO**
Lake Ohrid (9)	41.10	20.63	693	15.3	1019.1	0.3	24.9	Lake	Albania /North Macedonia	Publi.	Sadori et al.. (2016)	Digitised	**COST**	**TUND**
Torrecilla de Valmadrid (10)	41.45	-0.90	570	14.0	433.5	5.2	23.0	Colluvium	Spain	Publi.	Valero-Garces et al.. (2004)	Digitised	**WAMX**	**TUND**
Valle di Castiglione (11)	41.89	12.75	44	16.0	974.5	5.8	24.0	Lake	Italy	ACER	Follieri et al.. (1989)	Raw Count	**TEDE**	**TEFO**
Lake Estanya (12)	42.03	0.53	670	12.6	711.5	2.8	23.4	Lake	Spain	Publi.	Vegas-Villarubia et al.. (2013)	Digitised	**COST**	**TUND**
Stracciacappa (13)	42.13	12.32	220	14.5	850.2	5.8	23.3	Lake	Italy	ACER	Giardini. (2007)	Raw Count	**COST**	**TEFO**
Banyoles (14)	42.13	2.75	173	14.1	883.3	5.0	23.5	Lake	Spain	EPD (E#931)	Pérez-Obiol & Julia. (1994)	Raw Count	**COST**	**TEFO**

Lago di Monterosi (15)	42.22	12.43	237	15.0	1084.8	5.5	23.9	Lake	Italy	Publi.	Bonatti. (1970)	Raw Count	COST	TEFO
Lago Vico (16)	42.32	12.17	510	13.4	1086.2	4.6	22.7	Lake	Italy	Publi.	Magri & Sadori. (1999)	Digitised	WAST	TUND
Lagaccione (17)	42.57	11.85	355	14.1	867.9	4.8	22.7	Lake	Italy	ACER	Magri. (1999)	Raw Count	COST	TEFO
Freychinede (18)	42.78	1.43	1350	12.4	626.7	-1.6	20.3	Lake	France	Publi.	Jalut et al.. (1992)	Digitised	TUND	TUND
Dziguta (19)	42.99	41.07	35	11.0	1302.7	2.9	22.2	Peat Bog	Georgia	Publi.	Arslanov et al.. (2007)	Digitised	CLMX	TEFO
Lourdes (20)	43.03	-0.08	430	14.0	1619.2	0.9	17.1	Lake	France	Publi.	Reille & Andrieu. (1995)	Digitised	WAST	TUND
Tourbiere de l'Estarres (21)	43.09	-0.38	356	12.5	1078.9	3.4	17.3	Peat Bog	France	Publi.	Jalut et al.. (1988)	Digitised	COST	TEFO
Pian del Lago (22)	44.32	9.49	833	12.9	1034.3	6.1	21.3	Lake	Italy	Publi.	Guido et al.. (2020)	Digitised	COMX	TEFO
Lac du Bouchet B5 (23)	44.92	3.78	1200	12.2	1051.4	-0.4	19.4	Lake	France	Publi.	De Beaulieu et al.. (1990)	Digitised	COST	TUND
Lago della Costa (24)	45.27	11.74	7	8.3	1001.7	2.3	23.4	Lake	Italy	Publi.	Paganelli. (1996)	Digitised	COST	BOFO
Orgiano (25)	45.29	11.43	19	12.8	945.6	2.2	23.5	Peat Bog	Italy	Publi.	Miola et al.. (2006)	Digitised	COST	TEFO
Venice (26)	45.63	12.65	0	13.0	960.3	3.8	23.3	Peat Bog	Italy	ACER	Pini et al.. (2009)	Digitised	COST	TEFO
Azzano Decimo (27)	45.88	12.72	10	13.5	1145.4	2.4	22.7	Alluvial Fan	Italy	ACER	de Beaulieu & Reille. (1984)	Raw Count	COST	TEFO
Rio Doidis (28)	46.12	13.19	152	13.3	1299.7	1.0	21.0	Lake	Italy	Publi.	Monegato et al.. (2007)	Digitised	COST	STEP
Lake Sfanta Anna (29)	46.13	25.89	946	12.4	1500.9	-5.3	19.7	Lake	Romania	Publi.	Magyari et al.. (2014)	Digitised	COMX	TEFO

Travesio (30)	46.20	12.87	220	11.5	751.1	-0.6	19.7	Lake	Italy	Publi.	Monegato et al.. (2007)	Digitised	COST	WTFO
Billerio (31)	46.22	13.21	300	12.5	1662.2	-0.1	20.1	Lake	Italy	Publi.	Monegato et al.. (2007)	Digitised	TAIG	TEFO
Orvenco (32)	46.25	13.17	380	12.5	1634.6	-2.0	18.4	Alluvial Fan	Italy	Publi.	Monegato et al.. (2007)	Digitised	COST	STEP
Feher Lake (33)	46.45	20.65	86	13.4	1277.0	-0.5	22.7	Lake	Hungary	Publi.	Magyari et al.. (2014)	Raw Count	COST	TEFO
Kokad (34)	47.40	21.93	112	11.3	624.0	-1.3	21.8	Peat Bog	Hungary	Publi.	Magyari et al.. (2019)	Raw Count	COST	STEP
La Grande Pile (35)	47.73	6.50	330	10.5	692.1	1.3	19.0	Peat Bog	France	Publi.	de Beaulieu & Reille. (1989) + de Beaulieu (1992) + de Beaulieu & Reille (1992)	Raw Count	COST	TUND
Furamoos (36)	47.99	9.87	200	10.7	1141.5	-1.6	17.0	Lake	France	Publi.	Kern et al.. (2021)	Raw Count	COST	TUND
Bergsee (37)	47.57	7.94	382	8.2	1118.5	-0.3	18.3	Lake	Germany	Publi.	Duprat-Oualid et al.. (2017)	Digitised	COST	TUND
Pilsensee (38)	48.03	11.19	534	9.4	1306.8	-1.8	17.3	Lake	Germany	Publi.	Küster. (1995)	Digitised	COST	TUND
Nagymohos (39)	48.33	20.44	297	9.6	1110.5	-3.0	19.8	Peat Bog	Hungary	Publi.	Magyari et al.. (1999)	Raw Count	COST	TUND
Eifel (40)	50.30	6.51	565	9.5	751.6	-0.1	18.4	Lake	Germany	Publi.	Sirocko et al.. (2016)	Raw Count	COST	TEFO
La Grotte Walou (41)	50.59	5.54	252	10.9	922.2	1.9	17.3	Cave	Belgium	Publi.	Damblon. (2011)	Digitised	COST	TEFO
Kersdorf-Briesen (42)	52.33	14.27	44	9.2	657.2	-0.3	18.9	Lake	Germany	Publi.	Strahl. (2005)	Digitised	COST	TEFO
Mickunai (43)	54.72	25.53	143	6.3	650.0	-2.8	17.8	Lake	Lithuania	Publi.	Satkunas & Grigiene. (2012)	Digitised	COST	TEFO

***Table 1.** Reference table of fossil pollen data including (i) site locations and archives, (ii) modern annual and monthly climate data, and (iii) selected biomes and megabiomes derived from the European Centre for Medium-Range Weather Forecasts Reanalysis v5 (ERA5; from January 1940) for each site. These values are used to infer climate anomalies during the most climatically stable interval of the LGM (19–23 kyr). Green and blue lines indicate modified and additional pollen sites, respectively, relative to Davis et al. (2024). See **Fig.2** for definitions of biome and megabiome acronyms.*

III.2 - Age models

Age models previously based on CLAM v. 1.2 were updated using the Bayesian age-depth model Bacon (BACON routine in R, *Blaauw et al., 2010*). Radiocarbon ages were calibrated with the INTCAL20 calibration curve (*Reimer et al., 2020*). A linear accumulation/sedimentation rate was assumed over time to extend age models beyond the youngest and oldest available ^{14}C age ranges. In addition, ^{40}Ar age constraints were also included for the Füramoos fossil site. All ages are reported in calibrated years before 1950 (cal BP).

III.3 - Modern pollen and climate datasets

Calibrating with modern samples is advantageous because pollen data are highly resolved spatially, assumed to be largely free of preservation biases, and associated with directly measured climate variables. A modern dataset covering broad climatic gradients is required to provide a reliable calibration and ensure robust climate reconstructions (e.g., *Birks, 1995; Juggins, 2013*). The modern pollen training dataset used in this study has been compiled from the Eurasian Modern Pollen database v2 (EMPD2; https://empd2.github.io, https://www.pangaea.de/). It contains a total of 8,746 modern samples mostly across the Palearctic biogeographic realm, from Asia to Europe. The modern pollen dataset was harmonized using the same table used for the fossil pollen data (i.e., *LegacyPollen 2.0*). Modern climate variables associated with these modern pollen samples were extracted through nearest-neighbor interpolation from ERA5 reanalysis (https://rmets.onlinelibrary.wiley.com/doi/10.1002/qj.3803), at a spatial resolution of 30 seconds (i.e., 1 km^2), with temporal averages spanning from 1940 to present (*Hersbach et al., 2020*). We used monthly averages of daily mean data to extract the mean annual and seasonal climates (i.e., the coldest and warmest climate states of the year). The modern climate conditions at fossil site locations, extracted from the modern dataset and represented by colored points in **Appendix 1**, generally show latitudinal dependency, with warmer and drier climates concentrated at lower latitudes.

IV. Calibration methods

IV.1 - Local calibration methods from (mega)biomes

IV.1.1 - Modern calibration based on (mega)biomes

Modern datasets that cover extensive geographic regions (e.g., Europe) span a wide range of climatic conditions and are thus often challenging for reconstruction methods designed to estimate pollen-climate relationships (i.e., WA-PLS and CREST). In Europe, this difficulty is compounded by the underrepresentation of modern cold climates, limiting their use for reconstructing past cold conditions. The presence of such heterogeneity can reduce the ability of these methods to accurately match fossil samples with modern analogues. Without proper pre-processing of modern analogues, the performance, reliability, and robustness of reconstruction methods are compromised, potentially leading to less precise climate estimates (*Cao et al., 2022*).

Biomes are large-scale ecological units characterized by dominant vegetation types and the climatic and environmental conditions that support them (e.g., *Prentice et al., 1992, 1996*). They capture broad vegetation patterns and climate-vegetation relationships over space and time, facilitating comparisons across regions and temporal scales. Biomization processes prepare the data by classifying the pollen assemblages into PFTs and biomes, which are then used in reconstruction methods. *Guiot et al. (1993)* suggests using the biome approach of *Prentice et al. (1992)* to distinguish between steppe and tundra environments, thereby addressing the lack of good modern analogues.

In this study, biome and megabiome classification methods were applied to modern and fossil (LGM) European pollen assemblages. By processing a large European modern dataset (see ***section III.3***) through the biomization procedure, we minimize the risk of lacking analogues and integrate spatial heterogeneity of the modern samples to reconstruct regional vegetation patterns. The methodology for processing pollen data to extract climatic signals is illustrated in **Fig.1**.

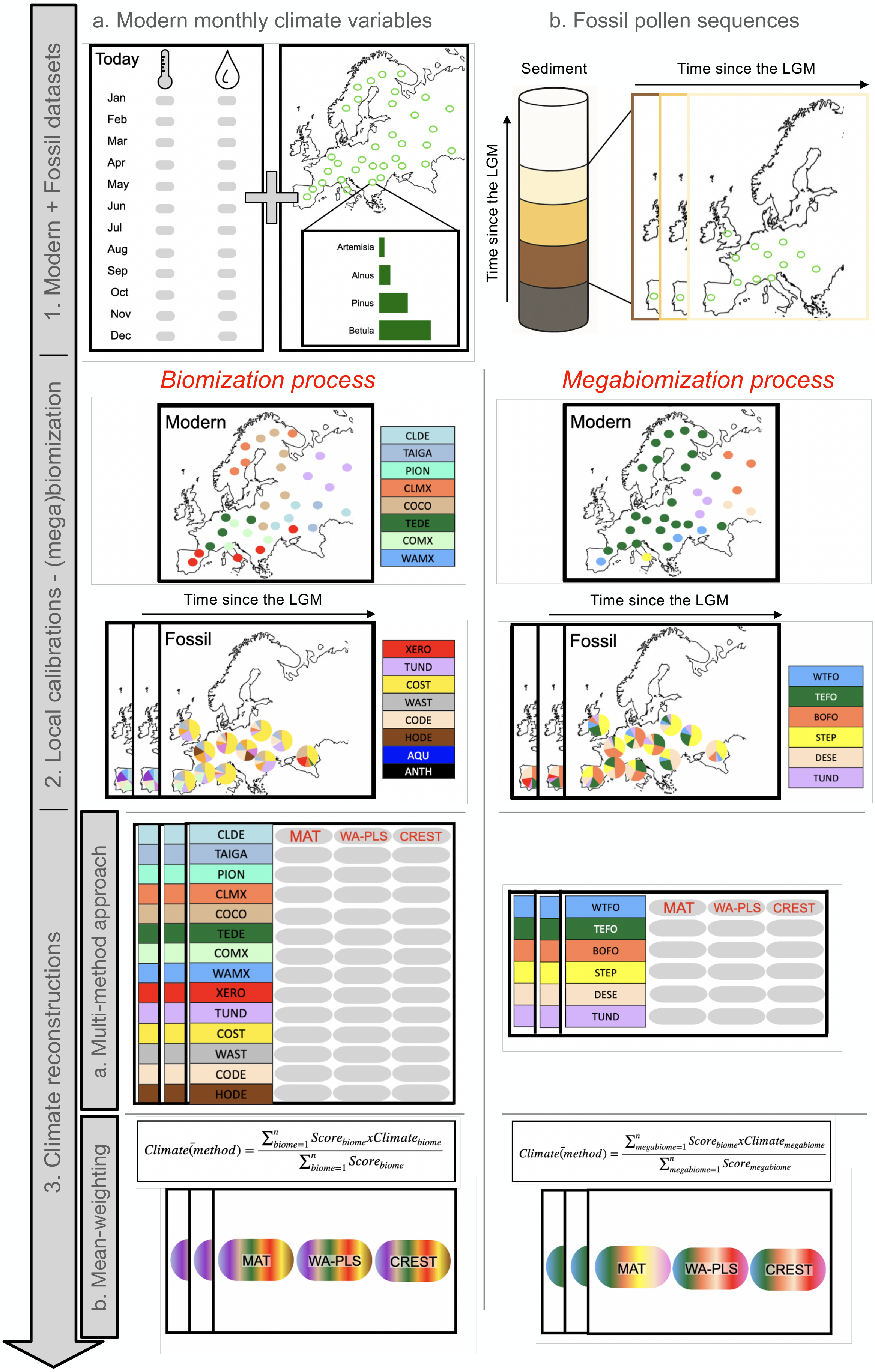
1. Modern + Fossil datasets
a. Modern monthly climate variables
b. Fossil pollen sequences
Today
Jan
Feb
Mar
Apr
May
Jun
Jul
Aug
Sep
Oct
Nov
Dec
Artemisia
Alnus
Pinus
Betula
Sediment
Time since the LGM
2. Local calibrations - (mega)biomization
Biomization process
Megabiomization process
Modern
Fossil
CLDE
TAIGA
PION
CLMX
COCO
TEDE
COMX
WAMX
XERO
TUND
COST
WAST
CODE
HODE
AQU
ANTH
WTFO
TEFO
BOFO
STEP
DESE
3. Climate reconstructions
a. Multi-method approach
b. Mean-weighting
MAT
WA-PLS
CREST
$Climate(method) = \frac{\sum_{biome=1}^{n} Score_{biome} x Climate_{biome}}{\sum_{biome=1}^{n} Score_{biome}}$
$Climate(method) = \frac{\sum_{megabiome=1}^{n} Score_{biome} x Climate_{megabiome}}{\sum_{megabiome=1}^{n} Score_{megabiome}}$

Figure 1. *Schematic representation of the methodological approach developed in the subsection II of this study. Gray vertical boxes (on the left of this figure) illustrate methodological steps performed in this study.*

IV.1.2 - Biomization procedure

Biomization was originally designed to reconstruct past vegetation patterns across specific regions of the world (e.g., Europe, Africa) for key periods such as the Mid-Holocene or the LGM (*Prentice et al. 1996*). This approach relies on a standardized methodology that uses modern and/or fossil pollen data (*Prentice and Webb, 1998; Prentice et al., 1996, 2000; Peyron et al., 1998*) and generally follows the sum of square root procedure (square-root transformation) to assign pollen taxa to biomes (*Prentice et al., 1996; Prentice and Webb, 1998*). Here, the taxa list defines PFTs following the European biomization scheme from *Peyron et al. (1998)* and *Tarasov et al. (2000).* A pollen abundance threshold of 0.5% (*Prentice et al., 1996*) - 0.2% for *Corylus* - is subtracted from the initial pollen taxon abundances to account for pollen transport effects (*Prentice et al., 1998*). Counts for *Larix* and *Pinus* were multiplied by factors of 15 and 0.5, respectively, to account for their specific levels of production (i.e., underproduction and low preservation) and pollen overproduction, respectively (*Bigelow et al., 2003; Binney et al., 2017*).

We assigned 98 pollen taxa to 25 PFTs (***Supp Mat.***, from *Prentice et al., 1996*), using the sum of the square roots of the pollen abundances corrected for thresholds. This approach allows for floristic and functional heterogeneity within key biomes. Then, biome affinity scores were calculated by considering the sum of the PFT scores belonging to each biome. Intermediate biomes (*Tarasov et al., 1998*) were used to distinguish warm and cold conditions from steppe and desert biomes by re-assigning PFT scores based on the dominant biome. Additionally, PFTs were combined into 16 biomes following *Prentice et al. (1996)* and using the standardized biome assignment procedure from *Harrison et al. (2010)* and *Dallmeyer et al. (2019).* The *Taxa-PFT* and *PFT-biome* biomization tables are available in **Supplementary materials (csv file)** with the following biomes: *cold deciduous forest (CLDE), taiga (TAIG), pioneer (PION), cold mixed forest (CLMX), cool conifer forest (COCO), temperate deciduous forest (TEDE), cool/warm mixed forest (COMX/WAMX), xerophytic shrubs (XERO), tundra (TUND), cool/warm steppes (COST/WAST), cold/hot desert (CODE/HODE), anthropogenic (ANTH), and aquatic (AQU) biomes.*

Biomization studies have considered three main hypotheses regarding the approach to (i) selecting the pollen-PFT assignment based on vegetation and environmental distributions from specific regions (*Prentice et al., 1996, 2000*), (ii) prioritizing the least PFT-rich biome when affinity values for multiple biomes are identical (*Harrison et al., 2010; Dallmeyer et al., 2019*) and (iii) choosing dominant biomes with the highest affinity score (absolute proportion of a particular biome) across different regions (*Xu et al., 2013*). Generally speaking, biomization also helps reduce the impact of the non-analogue effect (i.e., when modern samples are considered too different to the fossil ones to be used for reconstructions) on reconstructed climates.

IV.1.3 – Megabiomization procedure

Megabiomes are broad vegetation categories that group multiple biomes into larger ecological and climatic units (*Dallemeyer et al., 2019*). This classification, used alongside biomes in this study, relies on a more spatially extensive and global framework, yielding results that are more directly comparable to global vegetation models. Compared to the biomization procedure, only the content of the European classifications (linking taxa to PFTs and PFTs to biomes) is modified, while the methodology for calculating affinity scores remains the same. This classification aims to (i) define a small set of biomes (i.e., called megabiomes) based on shared PFTs, and (ii) cover a broader climatic range than individual biomes.

In this study, we used the megabiome classifications from *Dallmeyer et al. (2019)* and *Cao and Tian, (2021)*. The main aim of the PFTs–megabiome assignment is to track key signals of land-cover changes (e.g., wetland extent, conifer dominance) while minimizing the influence of the chosen biome classification (*Prentice et al., 1998*). Megabiome assignments are primarily used in some vegetation models (e.g., BIOME4, *Kaplan, 2003*), particularly when coupled with climate model simulations (as GCMs, *Haywood et al., 2009*). Affinity scores from pollen taxa were only calculated for pollen taxa percentages greater than 0.5% in order to increase signal-over-noise ratios (e.g., *Chen et al., 2010*), following the same scheme as that of the previously described biomization approach (see ***section IV.1.2***). For particular species, such as *Larix* and *Pinus*, we applied the same pollen production and transport corrections as described above for the biomization.

For Europe, 242 pollen taxa were grouped into PFTs and further assigned to 6 megabiomes (*Dallmeyer et al., 2019*): *temperate forest (TEFO), boreal forest (BOFO), warm-temperate forest (BOFO), tundra and polar desert (TUND), grassland and dry shrubland (STEP), and desert (DESE).* We directly used the algorithm implemented in R (*Cao and Tian, 2021*; R version 4.2.3, https://www.r-project.org/). When affinity scores were found equal, the megabiome with the fewest PFTs was selected. The correspondence of biome and megabiome tables are reported in **Appendix 2** for typical taxa in **Appendix 3**. **Table 2** summarizes pollen taxa to biome and megabiome assignment schemes used in this study.

Biome			
Taxa	PFTs	Biomes	Ref.
98	25	16	*Prentice et al., 1998*

Megabiome			
Taxa	PFTs	Megabiomes	Ref.
242	41	7	*Binney et al., 2017* *Marinova et al., 2018* *Cao et al., 2019*

Table 2. *Summary table of pollen taxa, plant functional types (PFTs), and (mega)biomes used in the biomisation frameworks, also provided in Supplementary Material 1.*

IV.2 - A weighted-mean approach to assess (mega)biome scores

One of the most notable issues of the (mega)biomization approaches is the sensitivity of reconstructed climates to small variations in biome scores (*Cruz-Silva et al., 2022*). The dominant biome effect (i.e., the biome with the highest affinity score) represents a significant source of uncertainty and poses major challenges for the reliability of reconstructed climate variables. This attribution of dominant (mega)biomes ignores potentially important (mega)biome contributions that are close to the maximum score and result in abrupt paleoclimate changes that merely reflect competition between (mega)biome scores rather than any significant bioclimatic shift.

To address this issue, we reconstruct fossil climate datasets for each (mega)biome using the three reconstruction methods (**section II**, MAT, WA-PLS, and CREST), distinguishing the modern calibration dataset (**section III.3**, EMPD2) by (mega)biome (biome-specific calibration datasets). We then calculate (mega)biome scores for each fossil sample and combine them with the climate reconstructions for each (mega)biome using a (mega)biome affinity score-weighted mean of climate variables (**Fig.1**). Finally, we evaluate the impact of using the (mega)biome affinity score-weighted mean approach of all fossil (mega)biome scores rather than relying solely on the dominant biome's climate signal.

V. Results

Vegetation and climate maps presented in this study use the WGS84 projection with coastal boundaries reflecting present-day conditions (**section III.3**). The LGM ice-sheet mask was obtained by combining data from *Peltier and Solheim (2004), Ehlers et al. (2011)* and *Seguinot et al. (2018)*. Climate reconstruction uncertainties of WA-PLS and MAT are provided as root mean square errors of prediction (RMSEP) derived from leave-one-out cross-validation.

V.1 – (Mega)biomization results: (mega)biome score processing

V.1.1 - Modern (mega)biome distribution maps

The modern distribution of biomes (from EMPD2 pollen dataset) across Eurasia shows that these are geographically homogeneous (**Fig 2.1.a**), with typical frequencies of biomes from 5% to 20% (**Fig 2.1.b**), except for cold deciduous forest (CLDE), desert (both cold (HODE) and hot HODE)) and supplementary biomes (pioneer (PION), anthropogenic (ANTH) and aquatic (AQU)), which are all minor (<1%) across Europe. Western Europe (e.g., France, Spain, Italy) exhibits the greatest biome diversity.

While cool conifer and cold mixed forests are primarily located in Scandinavia, cool mixed forests, taiga, and xerophytic woodlands surround the Mediterranean region. The warm mixed forest biome is dominant in southern Spain, Italy, and parts of the Near and Middle East. The clustering of different biomes in close geographic regions is attributed to broad climate patterns, altitude gradients, anthropogenic impacts (e.g., deforestation, agriculture, climate change), and/or local effects (e.g., proximity to water sources). The lack of data in Eastern Europe results in an underrepresentation of cold modern climate conditions.

Mean annual temperatures (TANN) are spatially variable in Europe and distinguished by (mega)biomes, reflecting ecological and climatic differences across regions (**Figs 2.1.c and 2.2.c**). TANN is generally negative in tundra regions (TUND, medians ~-9°C) and significantly higher in temperate forests (TEDE), cool mixed forests (COMX), warm mixed forests (WAMX), warm steppes (WAST), xerophytic woodlands (XERO), and hot deserts (HODE) (**Fig 2.1.b**). Other biomes, such as cold deciduous forests (CLDE), taiga (TAIG), pioneer (PION), cold mixed forests (CLMX), cool mixed forests (COMX), and cold steppes (COST), exhibit intermediate climatic conditions. The overlap of COMX and TEDE biomes in geographic and climatic spaces is likely due to their physiognomic similarities (*Binney et al., 2017*). As proposed by *Prentice et al. (1998)* and *Tarasov et al. (2000),* using the same biomization procedure as in this study, we observe a dominance of tundra and taiga in Russia, where modern conditions are among the driest in Europe.

The modern results derived from the major megabiome analysis (**Fig 2.2.a**) indicate a strong dominance of the temperate megabiome (TEDE) (~65%, **Fig 2.2.b**) across Europe, covering much of Western Europe and seemingly obscuring the greater diversity of biomes observed in **Fig 2.1.a**. While mountain regions exhibit a mix of CLMX, COMX, and COST biomes, the megabiomization analysis yields a predominance of TEDE, TUND and STEP (**Fig 2.1.b**). The climate space of the temperate megabiome (TEDE, **Fig 2.2.c**) is more arid (i.e., colder and drier) than the temperate biome (TEDE, **Fig 2.1.c**). Consequently, steppe megabiomes – including boreal forest (BOFO), grassland and dry shrubland (STEP), warm desert (DESE), and tundra and polar desert (TUND) - are sparse, although they share common locations with their modern biome counterparts (**Fig 2.2.c** and Table in **Appendix 2**).

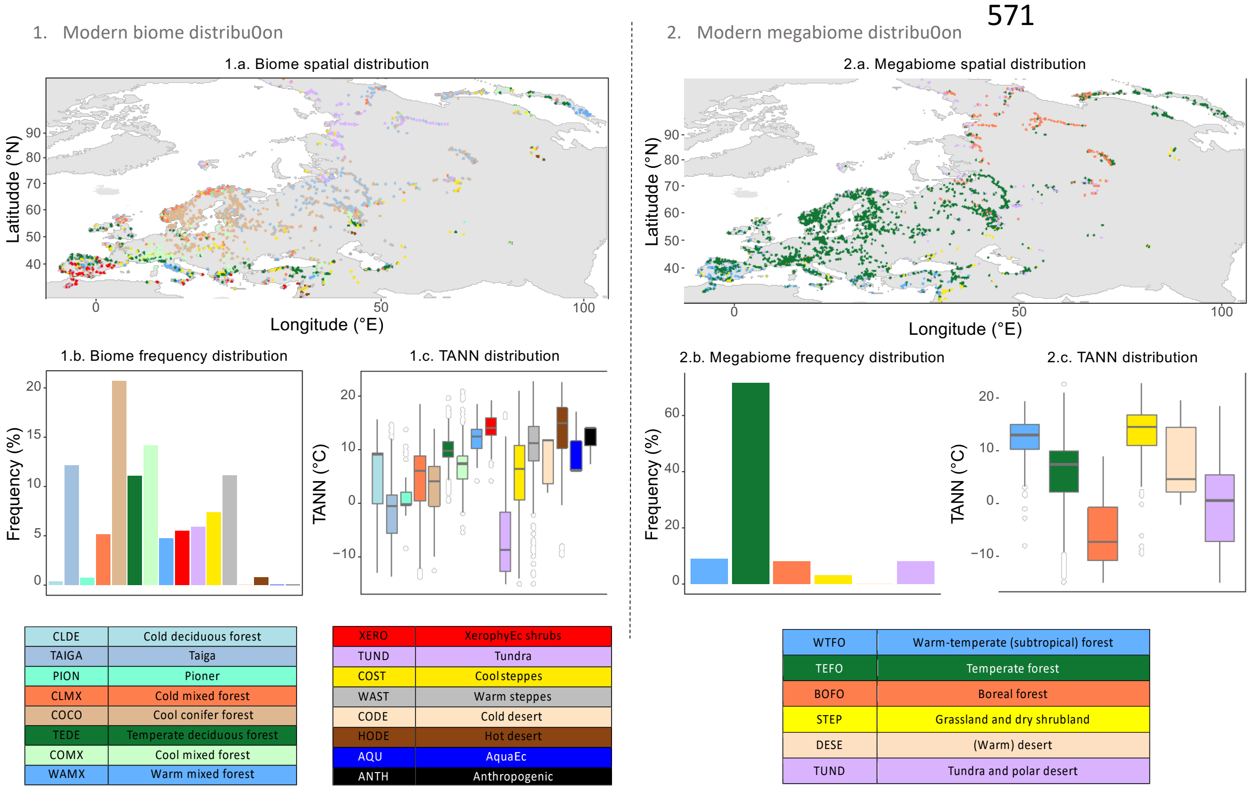

Figure 2. *European biome **(1)** and megabiome **(2)** spatial and modern climate distributions, using ECMWF Reanalysis v5 (ERA5; from January 1940, https://www.ecmwf.int/en/forecasts/dataset/ecmwf-reanalysis-v5) and EMPD2 dataset (Eurasian Modern Pollen Database, Davis et al., 2020). The biome classification, code and output database are available in **Supplementary materials**. The megabiome schema is described and in open access in Li et al., 2024, (https://doi.pangaea.de/10.1594/PANGAEA.965907). TANN = Mean Annual Temperature.*

V.1.2 - Fossil (mega)biomes during the LGM

LGM biome score results from the 43 selected European fossil sites reveal a clear dominance of the cool steppes, called COST (colored outlines around the pie charts from **Fig 3.a**). However, the dominant megabiome reconstructions oppose temperate (TEFO) and tundra and polar desert (TUND) megabiomes (**Fig 3.b**), with a few instances of steppic conditions around the Mediterranean region. In detail, (mega)biome scores of the LGM samples are very close to each other, indicating a strong competition and therefore only a weak dominance of any particular (mega)biome. For instance, while the total scores for arid megabiomes (i.e., grassland and dry shrubland (STEP) + desert (DESE) + tundra and polar desert (TUND)) range between 30% and 60%, these fossil sites remain dominated by the temperate megabiome, called TEDE (points with black outlines in **Appendix 4**). Even when one megabiome appears dominant during the LGM, several other megabiomes also display substantial scores. These results (**Figs 3.a and 3.b**) indicate an absence of a dominant vegetation ensemble, while transitional vegetation conditions are also apparent through the co-occurrence of multiple (mega)biomes. The selection of the dominant (mega)biome is thus based on marginal differences between competing scores, which underscores the limitation of this approach when several (mega)biomes co-exist within the same climatic period. By accounting for non-dominant (mega)biomes, our (mega)biome affinity score-weighted mean method based on (mega)biome scores can better capture underlying signals and provide more nuanced climate reconstructions across Europe.

By comparing biome and megabiome dominance scores, the steppic (STEP) and tundra (TUND) megabiomes - which correspond to the cold and hot steppic biomes (COST and WAST) and tundra (TUND) in **Appendix 2** - are not consistently observed, suggesting that the (mega)biome definitions (i.e., pollen and PFTs) in these two classification schemes reflect distinct climatic conditions (**Fig 1**). This therefore suggests that the choice of classification could influence the reconstructed climate conditions. The search for the best analogues across different climatic spaces grouped by (mega)biome highlights the challenges of distinguishing local climatic conditions and isolating LGM vegetation analogues for climate reconstructions at the European scale.

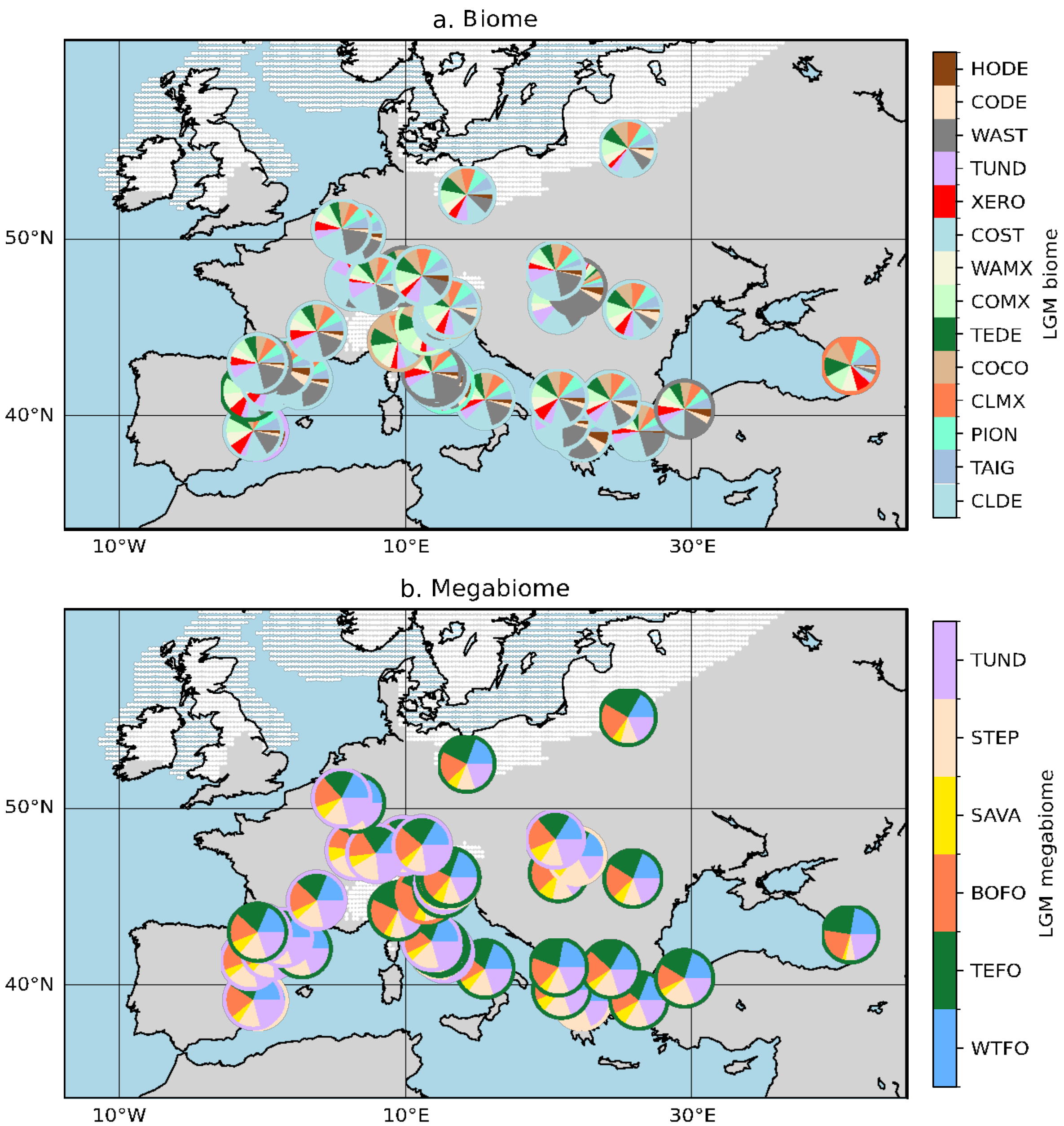

Figure 3. *Percentage of fossil biomes **(a)** and megabiomes **(b)** in pollen sequences during the LGM across Europe. Colored outlines around the pie charts indicate the dominant (mega)biomes. The white area represents the ice sheet extent.*

V.1.3 - (Mega)biome affinity score-weighted means

Mean annual temperature anomalies (i.e., $TANN_{reconstructed\ -\ Modern\ climate}$) over the past 40,000 years, obtained by combining the (mega)biomization and the three different reconstruction methods used in this study, are presented for the Lake Bouchet sequence in **Fig.4**. The near-zero climate anomalies observed for the present day at both sites confirm the accurate calibration of the reconstruction methods. TANN variations from both methods alternate between cold steppe (COST) and warm steppe (WAST) biomes (**Fig.3**) from 40 kyr to 10 kyr cal BP, before being mostly driven by temperate (TEDE) biomes from 10 kyr cal BP until present. Using the megabiome approach, we observe the same temperate (TEDE) dominance between 0 and 10 kyr cal BP, preceded by an alternation between tundra (TUND) and steppe (STEP) megabiomes from 40 kyr to 10 kyr cal BP. As shown in **Fig.3**, the COST biome and the TUND megabiome mainly dominate at Lake Bouchet during the LGM. The dominant (mega)biome method produces larger TANN variations due to alternance between these two co-dominant arid (mega)biomes, which correspond to distinct climatic conditions (**Fig 4**).

While the temporal variations in (mega)biome dominance at Lake Bouchet are comparable across reconstruction methods, the same (mega)biomes (i.e., based on identical modern and fossil sub-datasets) produce different TANN reconstructions depending on the method and calibration procedures (e.g., biomes vs. megabiomes) applied (**Fig.4**). The MAT method suggests strong instability in temperature (TANN) variations before 10 kyr cal BP, as a result of alternating dominant (mega)biomes. However, TANN variations appear synchronous and of similar amplitude (from -15 to 10°C) between biome and megabiome results from MAT (**Figs 4.a and 4.b**). In contrast, TANN variations derived from the WA-PLS (**Figs 4.c and 4.d**) and CREST (**Figs 4.e and 4.f**) methods indicate more stable climatic conditions that are consistent for a given classification. Nonetheless, TANN variations from WA-PLS and CREST are generally colder with the megabiome approach than with the biome approach (**Figs 4.e and 4.f**). Based on temperate (mega)biomes, TANN variations obtained with WA-PLS and CREST during the deglaciation gradient (10–0 kyr) show smaller extents of cooling using the biome rather than the megabiome procedure. While annual climatic conditions are similar between the megabiome (-3±3°C and -2±-1/-5°C, from WA-PLS and CREST methods, respectively) and the biome (-2±6°C and -1±5/-9°C, from WA-PLS and CREST methods, respectively) approach for WA-PLS and CREST during the LGM, the MAT method shows colder climatic conditions than the two other methods, with consistent values between the biome and megabiome approaches derived from MAT (-4±7°C and -6±3°C, respectively).

Due to the strong climatic instability predicted by MAT based on both biome and megabiome procedures, the (mega)biome affinity score-weighted mean approach appears to have the greatest impact on MAT-derived reconstructions (**Figs 4.a and 4.b**). All TANN variations derived from the biome affinity score-weighted mean approach show climatic changes that are synchronous with the results from the dominant (mega)biome approach, but with lower amplitudes. TANN variations from both the dominant and biome affinity score-weighted mean approaches exhibit LGM coolings, with amplitudes ranging from 2 to 8°C.

Most of the observed fluctuations in the modelled dominant vegetation (and therefore in the reconstructed climates) at Lake Bouchet thus arguably arise from a methodological limitation related to non-linear threshold effects, (mega)biome score competitions, and a high sensitivity of the estimation of dominant biomes to minor changes in vegetation assemblages. TANN reconstructed from biome affinity score-weighted means are less sensitive to this threshold effect as these transitions become gradual when including all the biome scores. The combination of these (mega)biome-specific climate reconstructions allows for more reliable and less noisy reconstructions, still capturing major climatic signals. This approach thus enhances the accuracy and robustness of pollen-based paleoclimate reconstructions by explicitly accounting for the uncertainties of (mega)biomization algorithms, representing a significant methodological advancement.

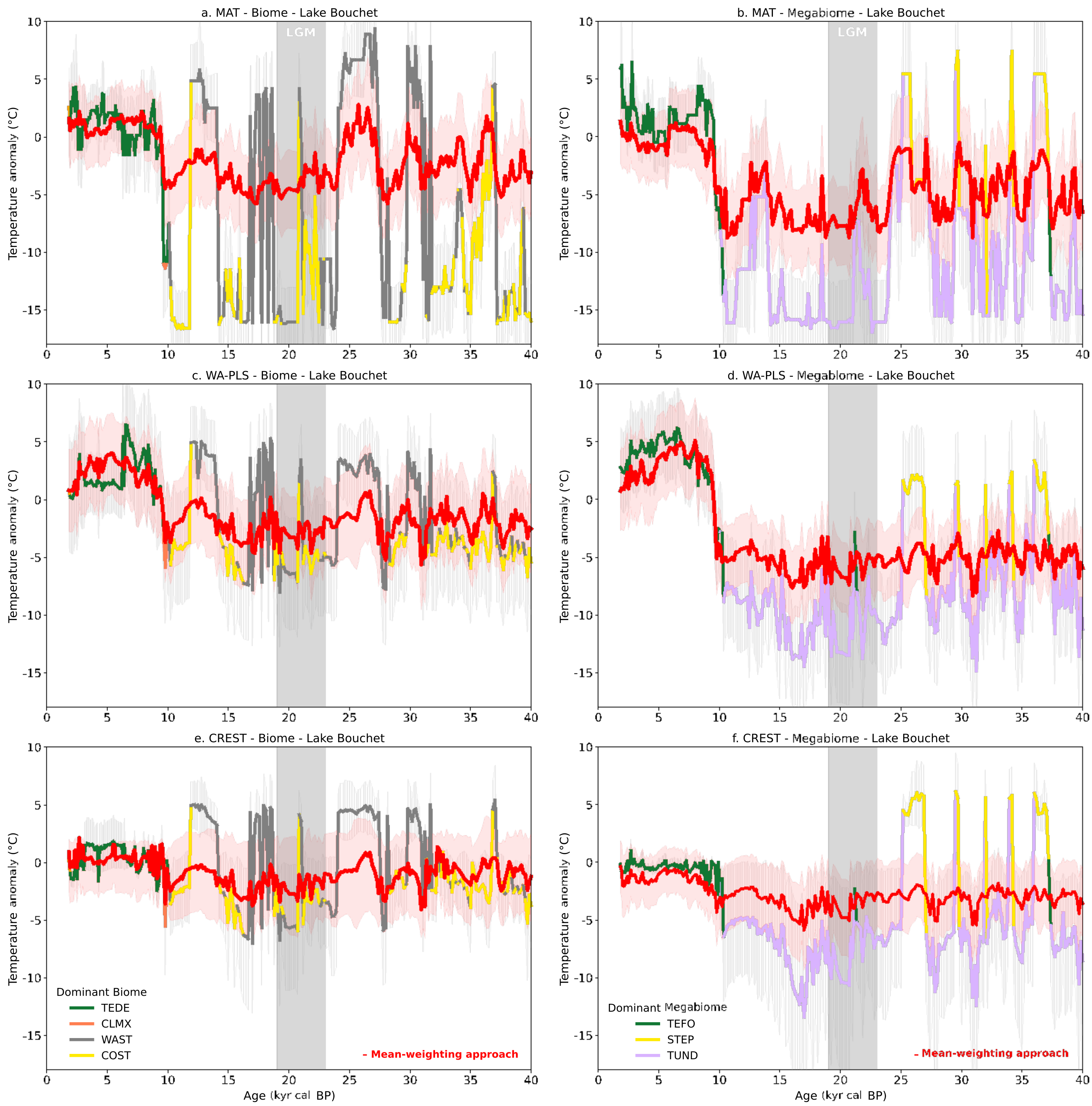

Figure 4. *TANN anomaly (LGM – Modern climate, LGM cooling) reconstructed over time at Lake Bouchet using three different reconstruction methods for (mega)biome procedures. Bold curves show TANN reconstructed and their climatic errors (1σ) from the dominant (mega)biome (colored according to the dominant biome). Bold red curves report the weighted mean TANN reconstructed from (mega)biome scores. Confidence in mean-weighting is indicated by red areas. The grey area indicates the LGM time interval. The modern climate reference is TANN = 8.3°C. All climate data were processed using the current biomization assignment scheme in CREST (**Fig.2**).*

V.2 – Multi-method temperature reconstructions using the (mega)biome affinity score-weighted mean approach during the LGM

V.2.1 - Cross-validation of the models

To assess the quality, performance and robustness of modeled climates using the three different methods, we apply a cross validation procedure from modern dominant biome datasets and show the existence of robust correlations (correlation, r) for TANN, Mean Temperature of the WArmest month (MTWA) and Mean Temperature of the COldest month (MTCO) in **Appendix 5**. Interestingly, the quality of the correlations of temperature reconstructions (including the three variables) using MAT and WA-PLS are generally similar across biomes, except for MAT correlations from the CLDE biome, which remain particularly low (r = 0.39, 0.41, and 0.55 for TANN, MTWA, and MTCO, respectively). The calibration dataset from the COST biome, which represents the dominant conditions of the LGM, shows good performances (r > 0.65 and RMSEP < 4.80°C) for both MAT and WA-PLS. Overall, biomes richest in PFTs (COCO, COMX, CLMX) show the strongest correlations (r > 0.7), consistent with previous findings by *Ortega-Rosas et al. 2008*. While megabiomes generally show less consistent performances than biomes, the DESE megabiome - the least dominant in both modern and fossil records - performs the worst (r < 0.46, from 12 modern samples).

By synthesizing the correlations and errors of the climatic variables across (mega)biomes (**Appendix 5**), we observe that all reconstruction methods reproduce the general trends of the modern climates reasonably well, with strong correlations (r > 0.6 on average, **Fig.5**). These high correlations are largely independent of the variable considered, as similar values are obtained for TANN, MTWA, and MTCO, suggesting that the methods capture the dominant climate gradients rather than being specifically sensitive to a given season. Among the methods, WAPLS consistently shows weaker correlations than MAT and CREST, indicating a lower ability to reproduce the modern climatic signals. In contrast, CREST correlations are less variable and remain tightly grouped (within ~0.1), which suggests greater robustness and stability compared to statistical transfer functions. Importantly, the average correlation values remain stable across calibration datasets, implying that the capacity of these methods to reproduce modern climate patterns is not significantly affected by the choice of (mega)biome calibration set.

Correlation metrics provide complementary insights into the absolute performance of the reconstruction methods in the error boxplot of **Fig.5**. On average, the three methods reproduce modern climate conditions with a mean error of approximately +3°C (RMSEP), which is generally acceptable for large-scale palaeoclimate reconstructions. However, a clear seasonal dependency emerges: winter temperatures (MTCO) are associated with larger errors (RMSEP≤ ±4.5°C in RMSEP), particularly when using MAT and CREST. This bias suggests that these methods struggle to capture the winter climatic conditions, possibly due to limitations in the underlying calibration data or in the sensitivity of the proxies to winter conditions. In contrast, summer (MTWA) and annual mean temperatures (TANN) are more precisely reconstructed across reconstruction methods, with the small errors around the mean.

The errors from global calibrations (in purple in **Fig.5**) are systematically higher than those obtained from (mega)biome calibrations. This observation suggests that calibration techniques from (mega)biomes increase the uncertainties in climate reconstructions. Error variability in the (mega)biomization procedure is larger across reconstruction methods than between the two calibration datasets (biomes). However, the quality and density of the calibration data, as well as the calibration techniques used, also influence the results and ultimately contribute to the uncertainties of the climate reconstructions.

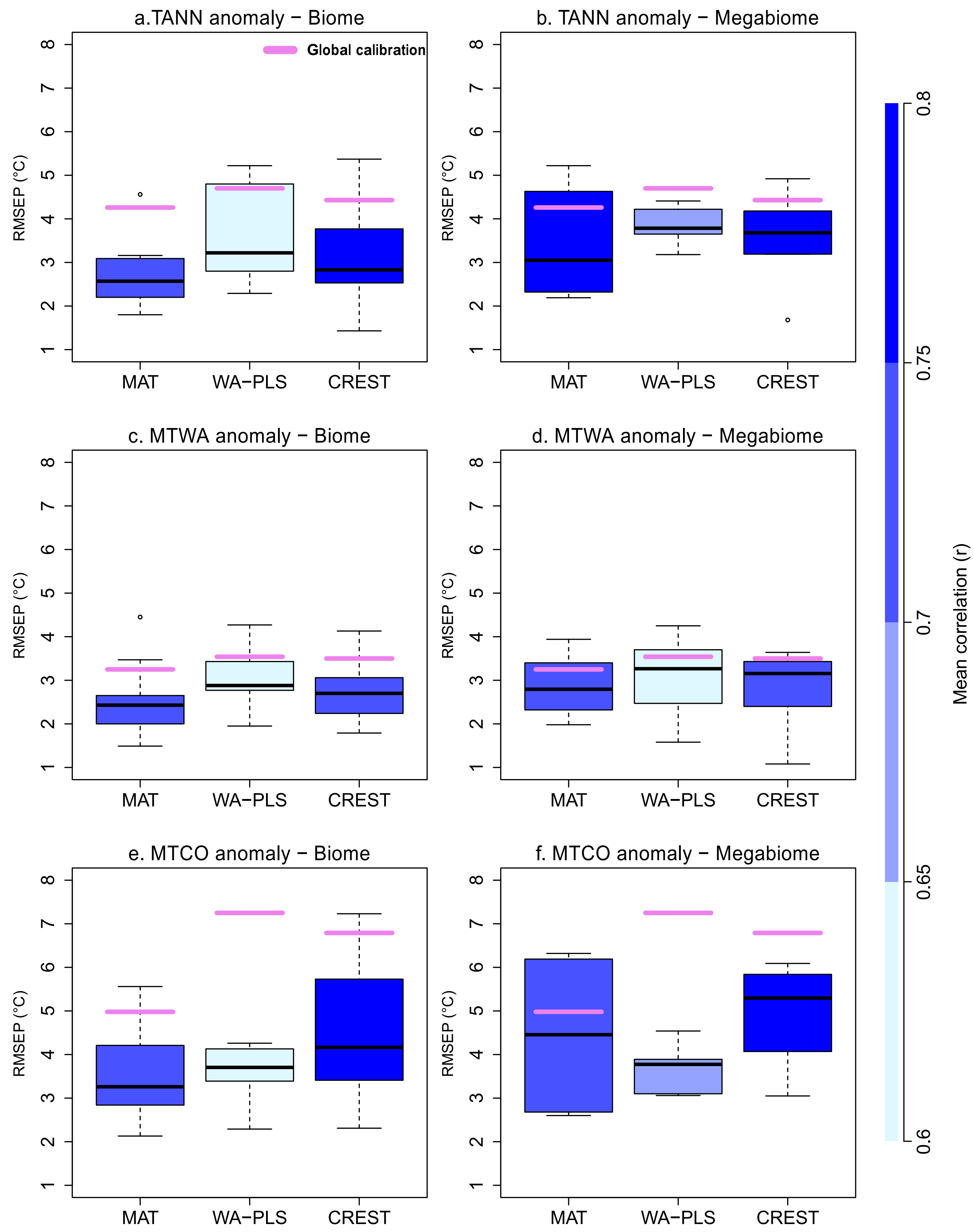

775 ***Figure 5.*** *Correlation boxplots of TANN **(a and d)**, MTWA **(b and e)** and MTCO **(c and f)** from*
776 *three different reconstruction methods using biomes and megabiomes, in first and second line,*

respectively. Reconstruction methods are indicated on the x-axis. Mean correlations (r) are reported in the common colorbar. The violet bars represent mean RMSEP values from the global calibration procedure. Results are reported ***Appendix 5****.*

V.2.2 – Annual temperature anomalies

LGM climate anomalies based on the (mega)biome affinity score-weighting approach and the three reconstruction methods are shown in **Fig.6** and summarized in **Table 3.** For the three different reconstruction methods, results at each core site are presented as anomalies compared to the modern climate estimated from ERA5-reanalysis (*Hersbach et al., 2020;* **Table 2**). From both vegetation classification methods, the LGM cooling across all fossil sites ranges from 1°C to 11°C, in line with LGM conditions significantly different from today. The mean European LGM cooling using the three reconstruction methods (MAT, WA-PLS, and CREST) yield 7.0±2.3°C, 7.1±2.2°C, and 5.9±2.2°C (mean SD, 1σ) from the biomization method (**Figs 6.a, 6.c and 6.d**) and 8.0±2.5°C, 7.2±2.4°C, and 7.0±2.3°C from the megabiomization method (**Figs 6.b, 6.d and 6.f**), respectively. The largest LGM coolings are observed in mountain ranges, such as the Alps and the Pyrenees (~10°C), with an agreement across all methods (standard deviation of ~1°C, **Appendix 6**). The Lake Bouchet (France), Kersdorf-Briesen (Germany) and Mickunai (Lithuania) fossil sites show the largest disagreement (~2°C standard deviation across the three methods). We could not detect any spatial gradient, or any influence of the proximity of the Fennoscandian ice-sheet from these two sets of reconstructions (i.e., biomization and megabiomization techniques, **Fig.6**).

a. Climate anomaly results from biomes | **Mean multi-method results**

	TANN MAT	TANN WA-PLS	TANN CREST	MTWA MAT	MTWA WA-PLS	MTWA CREST	MTCO MAT	MTCO WA-PLS	MTCO CREST	TANN	MTWA	MTCO
Lake Xinias	-8 ± 3	-8 ± 3	-6 ± -3 / -7	-8 ± 2	-5 ± 2	-5 ± -1 / -9	-5 ± 3	-6 ± 4	-4 ± -3 / -4	-7 ± -2 / -10	-6 ± -3 / -9	-5 ± -2 / -8
Cova de les Malladetes	-8 ± 3	-9 ± 4	-7 ± 1 / -9	-5 ± 3	-4 ± 3	-4 ± 7 / -12	-7 ± 4	-10 ± 6	-7 ± -5 / -7	-8 ± 2 / -11	-4 ± 2 / -10	-8 ± -4 / -12
Navarrés	-10 ± 3	-10 ± 3	-9 ± -2 / -9	-8 ± 3	-7 ± 3	-6 ± 3 / -14	-9 ± 5	-12 ± 5	-9 ± -8 / -11	-9 ± -1 / -12	-7 ± -1 / -12	-10 ± -6 / -14
Megali Limni	-11 ± 3	-12 ± 3	-8 ± -1 / -8	-9 ± 2	-8 ± 2	-8 ± 2 / -15	-17 ± 4	-18 ± 4	-11 ± -11 / -8	-10 ± -2 / -13	-8 ± -2 / -13	-15 ± -11 / -20
Ioannina	-6 ± 1	-7 ± 1	-5 ± -2 / -6	-4 ± 1	-3 ± 1	-2 ± 2 / -6	-2 ± 2	-4 ± 2	-1 ± -1 / -2	-6 ± -2 / -7	-3 ± 0 / -6	-3 ± -1 / -5
Lake Iznik	-6 ± 2	-6 ± 2	-5 ± 2 / -5	-6 ± 2	-4 ± 2	-4 ± 4 / -11	-6 ± 3	-7 ± 4	-5 ± -4 / -7	-5 ± 2 / -8	-5 ± 1 / -9	-6 ± -3 / -9
Lago Grande di Monticchio	-4 ± 1	-4 ± 1	-3 ± 0 / -3	-8 ± 1	-6 ± 1	-6 ± -2 / -9	-6 ± 1	-7 ± 1	-5 ± -5 / -6	-4 ± -1 / -5	-7 ± -4 / -9	-6 ± -5 / -7
Mire Straldzha Kupena-3	-5 ± 2	-5 ± 2	-4 ± 2 / -4	-8 ± 2	-8 ± 2	-8 ± 1 / -14	-13 ± 4	-11 ± 4	-9 ± -9 / -12	-5 ± 2 / -7	-8 ± -3 / -12	-11 ± -8 / -15
Lake Ohrid	-7 ± 2	-7 ± 2	-5 ± 1 / -7	-7 ± 2	-5 ± 2	-5 ± 4 / -12	-2 ± 3	-3 ± 3	0 ± 1 / -1	-7 ± 1 / -9	-6 ± 0 / -10	-2 ± 1 / -5
Torrecilla de Valmadrid	-4 ± 3	-5 ± 3	-5 ± 2 / -7	-5 ± 3	-3 ± 3	-4 ± 7 / -12	-4 ± 3	-7 ± 4	-6 ± -5 / -4	-5 ± 4 / -7	-4 ± 3 / -9	-5 ± -2 / -9
Valle di Castiglione	-6 ± 4	-7 ± 4	-7 ± 3 / -9	-6 ± 3	-5 ± 3	-5 ± 9 / -17	-4 ± 5	-7 ± 5	-7 ± -6 / -10	-7 ± 5 / -10	-5 ± 3 / -13	-6 ± -2 / -11
Lake Estanya	-5 ± 3	-5 ± 3	-3 ± 5 / -6	-6 ± 3	-5 ± 3	-4 ± 8 / -14	-5 ± 5	-6 ± 5	-3 ± -1 / -4	-5 ± 5 / -8	-5 ± 2 / -11	-5 ± 0 / -9
Stracciacappa	-6 ± 4	-7 ± 4	-6 ± 5 / -6	-4 ± 4	-4 ± 4	-4 ± 11 / -16	-9 ± 6	-10 ± 6	-8 ± -7 / -13	-7 ± 7 / -10	-4 ± 5 / -12	-9 ± -4 / -15
Banyoles	-8 ± 1	-7 ± 1	-6 ± -4 / -6	-5 ± 1	-4 ± 1	-4 ± -1 / -7	-11 ± 1	-10 ± 1	-7 ± -7 / -8	-7 ± -4 / -8	-5 ± -3 / -6	-10 ± -8 / -11
Lago di Monterosi	-10 ± 3	-11 ± 3	-10 ± -2 / -11	-7 ± 2	-7 ± 2	-8 ± 3 / -16	-13 ± 4	-14 ± 4	-11 ± -10 / -17	-10 ± -1 / -13	-7 ± -1 / -12	-12 ± -9 / -17
Lago Vico	-6 ± 2	-6 ± 2	-5 ± -1 / -5	-5 ± 1	-3 ± 1	-4 ± 2 / -8	-8 ± 2	-9 ± 2	-7 ± -7 / -8	-6 ± -1 / -7	-4 ± 0 / -7	-8 ± -6 / -10
Lagaccione	-7 ± 3	-7 ± 3	-6 ± -2 / -6	-5 ± 2	-4 ± 2	-4 ± 2 / -8	-8 ± 4	-10 ± 4	-7 ± -7 / -9	-7 ± -1 / -9	-4 ± -1 / -7	-8 ± -5 / -11

Freychinede	-7 ± 4	-6 ± 5	-4 ± 5 / -5	-3 ± 4	-3 ± 4	-3 ± 10 / -13	-8 ± 7	-6 ± 6	-2 ± -2 / -7	-6 ± 6 / -10	-3 ± 5 / -10	-5 ± 0 / -12
Dziguta	-8 ± 3	-9 ± 3	-6 ± 0 / -7	-6 ± 3	-4 ± 3	-4 ± 6 / -12	-8 ± 4	-10 ± 4	-4 ± -4 / -2	-8 ± 0 / -10	-5 ± 1 / -10	-8 ± -3 / -12
Lourdes	-5 ± 2	-6 ± 2	-5 ± -1 / -5	-1 ± 2	1 ± 1	1 ± 6 / -3	-2 ± 2	-5 ± 3	-4 ± -4 / -5	-5 ± -1 / -7	0 ± 4 / -2	-4 ± -1 / -6
Tourbiere de l'Estarres	-8 ± 3	-7 ± 3	-5 ± 2 / -5	-2 ± 3	0 ± 3	0 ± 10 / -7	-7 ± 4	-7 ± 5	-5 ± -4 / -3	-7 ± 2 / -9	-1 ± 6 / -6	-6 ± -3 / -11
Pian del Lago	-8 ± 2	-8 ± 2	-6 ± -1 / -6	-6 ± 2	-5 ± 2	-5 ± 3 / -11	-12 ± 3	-14 ± 4	-9 ± -9 / -12	-7 ± -1 / -9	-5 ± 0 / -9	-12 ± -8 / -15
Lac du Bouchet B5	-4 ± 1	-2 ± 1	-1 ± 2 / -1	-3 ± 1	-1 ± 1	-1 ± 3 / -5	-7 ± 2	-5 ± 2	-2 ± -2 / -3	-2 ± 1 / -4	-2 ± 1 / -4	-5 ± -2 / -7
Lago della Costa	-11 ± 2	-9 ± 2	-7 ± -2 / -8	-11 ± 2	-7 ± 2	-7 ± 1 / -13	-10 ± 3	-11 ± 3	-7 ± -7 / -11	-9 ± -3 / -11	-8 ± -3 / -13	-9 ± -6 / -13
Orgiano	-12 ± 3	-11 ± 3	-10 ± -5 / -9	-11 ± 3	-8 ± 3	-8 ± 0 / -15	-12 ± 5	-13 ± 5	-9 ± -12 / -5	-11 ± -4 / -14	-9 ± -4 / -14	-11 ± -7 / -16
Venice	-10 ± 3	-10 ± 3	-10 ± -4 / -13	-10 ± 3	-8 ± 3	-8 ± 2 / -16	-10 ± 4	-12 ± 5	-11 ± -9 / -18	-10 ± -3 / -13	-9 ± -3 / -14	-11 ± -7 / -16
Azzano Decimo	-8 ± 3	-9 ± 3	-10 ± -3 / -13	-8 ± 3	-6 ± 2	-7 ± 2 / -13	-6 ± 4	-10 ± 4	-11 ± -9 / -17	-9 ± -1 / -12	-7 ± -1 / -11	-9 ± -5 / -14
Rio Doidis	-4 ± 5	-6 ± 4	-6 ± 3 / -9	-4 ± 4	-3 ± 3	-3 ± 8 / -12	-2 ± 7	-5 ± 6	-6 ± -6 / -13	-5 ± 6 / -9	-3 ± 4 / -9	-5 ± 1 / -11
Lake Sfanta Anna	-9 ± 3	-9 ± 3	-8 ± -3 / -8	-8 ± 2	-5 ± 2	-4 ± 3 / -10	-1 ± 3	-4 ± 4	-1 ± 1 / -5	-9 ± -3 / -11	-6 ± -1 / -10	-2 ± 2 / -6
Travesio	-11 ± 3	-10 ± 3	-8 ± -3 / -7	-8 ± 3	-5 ± 3	-4 ± 4 / -11	-7 ± 4	-8 ± 4	-5 ± -6 / -1	-10 ± -3 / -12	-6 ± 0 / -11	-7 ± -3 / -11
Billerio	-9 ± 3	-9 ± 3	-8 ± -3 / -7	-7 ± 3	-4 ± 3	-4 ± 5 / -11	-5 ± 5	-8 ± 4	-5 ± -7 / -1	-9 ± -2 / -11	-5 ± 0 / -10	-6 ± -2 / -11
Orvenco	-11 ± 3	-10 ± 3	-9 ± -4 / -8	-7 ± 3	-3 ± 3	-3 ± 6 / -10	-4 ± 4	-6 ± 4	-3 ± -5 / 1	-10 ± -3 / -13	-4 ± 2 / -9	-5 ± -1 / -9
Feher Lake	-6 ± 2	-7 ± 2	-6 ± -3 / -7	-7 ± 2	-6 ± 2	-6 ± -1 / -11	-4 ± 3	-7 ± 3	-5 ± -5 / -8	-6 ± -2 / -8	-6 ± -3 / -9	-5 ± -3 / -9
Kokad	-5 ± 6	-6 ± 5	-6 ± 3 / -8	-7 ± 5	-6 ± 4	-6 ± 7 / -15	-2 ± 7	-6 ± 7	-6 ± -5 / -13	-6 ± 6 / -10	-6 ± 2 / -13	-5 ± 2 / -12
La Grande Pile	-6 ± 2	-6 ± 2	-5 ± -1 / -5	-4 ± 1	-3 ± 1	-2 ± 2 / -6	-6 ± 2	-7 ± 2	-5 ± -5 / -7	-5 ± -1 / -7	-3 ± 0 / -6	-6 ± -4 / -8
Furamoos	-4 ± 2	-5 ± 2	-4 ± 1 / -5	-4 ± 1	-2 ± 1	-1 ± 5 / -6	-3 ± 2	-7 ± 2	-4 ± -4 / -8	-4 ± 1 / -6	-2 ± 2 / -6	-5 ± -2 / -8
Bergsee	-5 ± 2	-6 ± 2	-6 ± -1 / -7	-3 ± 2	-4 ± 2	-3 ± 4 / -8	-6 ± 3	-8 ± 4	-6 ± -5 / -10	-6 ± 0 / -8	-3 ± 1 / -7	-6 ± -4 / -10
Pilsensee	-7 ± 3	-7 ± 4	-6 ± -1 / -4	-4 ± 3	-3 ± 3	-2 ± 6 / -9	-5 ± 4	-6 ± 5	-5 ± -6 / 0	-7 ± 0 / -9	-3 ± 2 / -8	-5 ± -1 / -10
Nagymohos	-6 ± 2	-6 ± 2	-5 ± -1 / -6	-5 ± 2	-4 ± 2	-4 ± 1 / -8	-4 ± 3	-5 ± 3	-2 ± -2 / -5	-6 ± -1 / -7	-4 ± -1 / -7	-4 ± -2 / -7
Eifel	-5 ± 1	-7 ± 2	-4 ± 2 / -5	-3 ± 1	-2 ± 1	0 ± 7 / -6	-3 ± 2	-7 ± 2	-4 ± -4 / -8	-5 ± 1 / -7	-2 ± 3 / -5	-5 ± -2 / -8
La Grotte Walou	-5 ± 4	-5 ± 3	-4 ± 4 / -3	-3 ± 3	0 ± 3	1 ± 11 / -7	-3 ± 5	-6 ± 5	-5 ± -4 / -2	-5 ± 4 / -7	-1 ± 6 / -6	-5 ± -1 / -9
Kersdorf-Briesen	-7 ± 3	-6 ± 3	-5 ± 2 / -7	-7 ± 3	-4 ± 3	-3 ± 7 / -11	-7 ± 4	-7 ± 5	-5 ± -4 / -10	-6 ± 2 / -9	-5 ± 2 / -10	-6 ± -2 / -11
Mickunai	-3 ± 4	-1 ± 4	0 ± 8 / -1	-3 ± 4	-2 ± 4	-2 ± 10 / -12	-6 ± 6	-2 ± 6	1 ± 1 / -3	-1 ± 8 / -5	-3 ± 5 / -9	-3 ± 3 / -8
Mean population SD	-7 ± 2	-7 ± 2	-6 ± 2	-6 ± 2	-4 ± 2	-4 ± 2	-7 ± 4	-8 ± 3	-6 ± 3	-7 ± 2	-5 ± 2	-7 ± 3

b. Climate anomaly results from megabiomes | **Mean multi-method results**

	TANN MAT	TANN WA-PLS	TANN CREST	MTWA MAT	MTWA WA-PLS	MTWA CREST	MTCO MAT	MTCO WA-PLS	MTCO CREST	TANN	MTWA	MTCO
Lake Xinias	-10 ± 2	-8 ± 2	-8 ± -6 / -9	-8 ± 1	-4 ± 1	-4 ± -2 / -5	-3 ± 2	-8 ± 2	-7 ± -4 / -8	-9 ± -5 / -10	-5 ± -3 / -7	-6 ± -3 / -9
Cova de les Malladetes	-9 ± 4	-8 ± 4	-8 ± -4 / -11	-8 ± 3	-2 ± 3	-2 ± 2 / -4	-4 ± 6	-10 ± 5	-10 ± -4 / -14	-8 ± -1 / -12	-4 ± 0 / -8	-8 ± -2 / -14
Navarrés	-12 ± 3	-10 ± 3	-10 ± -6 / -13	-8 ± 2	-7 ± 2	-6 ± -2 / -8	-11 ± 4	-12 ± 4	-12 ± -6 / -16	-11 ± -5 / -13	-7 ± -4 / -9	-12 ± -7 / -16
Megali Limni	-13 ± 5	-12 ± 4	-12 ± -6 / -15	-11 ± 4	-9 ± 3	-9 ± -4 / -11	-14 ± 6	-17 ± 6	-15 ± -8 / -19	-12 ± -4 / -16	-10 ± -6 / -13	-15 ± -9 / -21
Ioannina	-8 ± 2	-7 ± 2	-6 ± -4 / -7	-5 ± 1	-3 ± 1	-2 ± 0 / -3	-1 ± 2	-5 ± 2	-3 ± 0 / -5	-7 ± -4 / -9	-3 ± -1 / -5	-3 ± 0 / -6
Lake Iznik	-7 ± 3	-5 ± 3	-5 ± -2 / -7	-7 ± 2	-2 ± 2	-3 ± 1 / -5	-2 ± 4	-7 ± 4	-6 ± -1 / -9	-6 ± 0 / -9	-4 ± -1 / -7	-5 ± 0 / -10
Lago Grande di Monticchio	-6 ± 1	-4 ± 1	-4 ± -2 / -5	-9 ± 1	-6 ± 1	-5 ± -4 / -6	-4 ± 2	-7 ± 2	-6 ± -4 / -8	-4 ± -2 / -6	-7 ± -5 / -8	-6 ± -4 / -8
Mire Straldzha Kupena-3	-7 ± 3	-7 ± 3	-6 ± -2 / -8	-8 ± 2	-8 ± 3	-6 ± -3 / -8	-10 ± 4	-16 ± 5	-14 ± -7 / -17	-7 ± 0 / -10	-7 ± -4 / -10	-13 ± -7 / -18
Lake Ohrid	-9 ± 3	-7 ± 3	-7 ± -3 / -9	-8 ± 2	-5 ± 2	-4 ± -1 / -6	0 ± 4	-3 ± 4	-3 ± 3 / -5	-8 ± -2 / -10	-6 ± -3 / -9	-2 ± 3 / -6
Torrecilla de Valmadrid	-6 ± 3	-4 ± 4	-5 ± -1 / -8	-6 ± 3	-2 ± 3	-2 ± 2 / -4	-2 ± 5	-5 ± 5	-8 ± -1 / -11	-5 ± 2 / -8	-3 ± 1 / -6	-5 ± 1 / -10
Valle di Castiglione	-6 ± 5	-7 ± 5	-8 ± -1 / -12	-5 ± 4	-4 ± 4	-4 ± 2 / -7	-1 ± 7	-7 ± 8	-10 ± 0 / -16	-7 ± 3 / -12	-4 ± 1 / -8	-6 ± 3 / -14
Lake Estanya	-7 ± 5	-4 ± 4	-5 ± 0 / -8	-7 ± 3	-4 ± 3	-3 ± 2 / -6	-3 ± 6	-5 ± 6	-7 ± 0 / -10	-5 ± 3 / -10	-5 ± -1 / -8	-5 ± 2 / -11
Stracciacappa	-8 ± 6	-7 ± 5	-7 ± 0 / -11	-6 ± 4	-3 ± 4	-3 ± 3 / -7	-5 ± 8	-12 ± 8	-11 ± -1 / -17	-8 ± 3 / -13	-4 ± 1 / -8	-9 ± 0 / -17
Banyoles	-10 ± 1	-7 ± 1	-7 ± -6 / -8	-7 ± 1	-4 ± 1	-4 ± -2 / -4	-8 ± 2	-11 ± 2	-9 ± -7 / -10	-8 ± -6 / -10	-5 ± -3 / -6	-9 ± -7 / -11
Lago di Monterosi	-12 ± 4	-12 ± 4	-12 ± -6 / -15	-7 ± 3	-6 ± 3	-7 ± -2 / -10	-11 ± 5	-17 ± 6	-15 ± -7 / -20	-12 ± -4 / -16	-7 ± -3 / -10	-15 ± -8 / -21
Lago Vico	-9 ± 2	-6 ± 2	-7 ± -4 / -8	-6 ± 1	-3 ± 2	-3 ± -1 / -4	-7 ± 3	-9 ± 3	-10 ± -6 / -12	-7 ± -3 / -9	-4 ± -2 / -6	-9 ± -5 / -12

Lagaccione	-9 ± 2	-7 ± 2	-8 ± -5 / -9	-6 ± 1	-3 ± 1	-3 ± -1 / -4	-7 ± 3	-10 ± 3	-10 ± -7 / -12	-8 ± -4 / -10	-4 ± -2 / -6	-9 ± -6 / -12
Freychinede	-7 ± 5	-7 ± 5	-6 ± 1 / -10	-3 ± 4	-2 ± 4	-1 ± 5 / -4	-1 ± 7	-8 ± 8	-6 ± 3 / -12	-7 ± 3 / -11	-2 ± 3 / -6	-5 ± 3 / -13
Dziguta	-11 ± 3	-8 ± 4	-8 ± -3 / -10	-6 ± 2	-4 ± 3	-4 ± 0 / -6	-10 ± 5	-10 ± 5	-7 ± -1 / -10	-9 ± -2 / -12	-5 ± -1 / -7	-9 ± -3 / -14
Lourdes	-7 ± 2	-6 ± 2	-6 ± -3 / -7	-1 ± 1	1 ± 2	1 ± 4 / 0	-1 ± 3	-7 ± 3	-5 ± -1 / -7	-6 ± -3 / -8	0 ± 2 / -2	-4 ± 0 / -7
Tourbiere de l'Estarres	-9 ± 4	-6 ± 4	-6 ± -1 / -9	-2 ± 3	1 ± 3	1 ± 6 / -1	-5 ± 5	-8 ± 5	-6 ± 0 / -10	-7 ± 0 / -11	0 ± 4 / -3	-6 ± 0 / -11
Pian del Lago	-8 ± 3	-8 ± 3	-7 ± -3 / -9	-5 ± 2	-5 ± 3	-4 ± -1 / -6	-10 ± 4	-15 ± 5	-12 ± -7 / -15	-8 ± -2 / -10	-5 ± -2 / -7	-12 ± -7 / -16
Lac du Bouchet B5	-6 ± 2	-3 ± 2	-2 ± 0 / -3	-5 ± 1	-1 ± 1	-1 ± 1 / -2	-5 ± 2	-7 ± 2	-4 ± -2 / -6	-4 ± 0 / -6	-2 ± 0 / -4	-6 ± -3 / -8
Lago della Costa	-12 ± 3	-10 ± 3	-9 ± -5 / -11	-10 ± 2	-8 ± 3	-6 ± -2 / -8	-9 ± 4	-12 ± 5	-10 ± -4 / -13	-10 ± -4 / -13	-8 ± -4 / -11	-10 ± -5 / -14
Orgiano	-11 ± 3	-10 ± 4	-10 ± -5 / -13	-11 ± 3	-9 ± 3	-7 ± -3 / -9	-7 ± 5	-12 ± 6	-11 ± -5 / -15	-11 ± -4 / -14	-9 ± -5 / -12	-10 ± -4 / -15
Venice	-11 ± 5	-11 ± 4	-10 ± -5 / -14	-9 ± 3	-7 ± 3	-6 ± -1 / -9	-11 ± 6	-16 ± 6	-13 ± -5 / -18	-11 ± -3 / -15	-7 ± -3 / -11	-13 ± -6 / -19
Azzano Decimo	-10 ± 4	-11 ± 4	-10 ± -5 / -14	-8 ± 3	-6 ± 3	-6 ± -2 / -9	-5 ± 5	-13 ± 6	-12 ± -4 / -17	-10 ± -3 / -14	-7 ± -3 / -10	-10 ± -3 / -17
Rio Doidis	-6 ± 5	-6 ± 4	-6 ± 0 / -11	-5 ± 3	-1 ± 3	-2 ± 4 / -5	3 ± 7	-8 ± 6	-8 ± 2 / -14	-6 ± 3 / -11	-2 ± 2 / -6	-4 ± 5 / -12
Lake Sfanta Anna	-9 ± 3	-8 ± 3	-8 ± -4 / -10	-6 ± 2	-4 ± 3	-3 ± 1 / -5	0 ± 4	-4 ± 5	-2 ± 3 / -5	-8 ± -2 / -11	-4 ± -1 / -7	-2 ± 3 / -6
Travesio	-11 ± 3	-9 ± 4	-8 ± -4 / -10	-6 ± 3	-4 ± 3	-3 ± 1 / -5	-5 ± 4	-8 ± 6	-6 ± 1 / -9	-9 ± -3 / -13	-4 ± -1 / -7	-6 ± -1 / -11
Billerio	-8 ± 3	-8 ± 4	-7 ± -3 / -10	-5 ± 3	-3 ± 3	-2 ± 2 / -4	-3 ± 5	-8 ± 5	-6 ± 0 / -10	-8 ± -1 / -11	-4 ± 0 / -6	-6 ± 0 / -11
Orvenco	-12 ± 4	-10 ± 4	-9 ± -5 / -12	-6 ± 3	-3 ± 3	-2 ± 3 / -4	-5 ± 5	-7 ± 5	-5 ± 1 / -8	-10 ± -4 / -14	-4 ± 0 / -7	-6 ± 0 / -11
Feher Lake	-6 ± 2	-7 ± 2	-7 ± -4 / -8	-7 ± 2	-6 ± 2	-5 ± -3 / -7	-2 ± 3	-8 ± 3	-6 ± -2 / -8	-7 ± -2 / -9	-6 ± -4 / -8	-5 ± -1 / -9
Kokad	-8 ± 7	-9 ± 5	-9 ± -1 / -14	-8 ± 5	-7 ± 4	-6 ± 0 / -10	-3 ± 8	-10 ± 8	-9 ± 3 / -16	-8 ± 3 / -14	-7 ± -2 / -11	-7 ± 3 / -16
La Grande Pile	-5 ± 2	-6 ± 2	-5 ± -3 / -6	-4 ± 1	-3 ± 1	-2 ± 0 / -3	0 ± 2	-9 ± 3	-6 ± -3 / -8	-6 ± -2 / -7	-3 ± -1 / -4	-5 ± -1 / -9
Furamoos	-5 ± 3	-7 ± 3	-5 ± -1 / -7	-2 ± 2	-2 ± 2	-1 ± 2 / -2	-3 ± 4	-10 ± 4	-7 ± -2 / -10	-6 ± 0 / -8	-2 ± 1 / -4	-7 ± -1 / -12
Bergsee	-5 ± 3	-6 ± 3	-6 ± -2 / -9	-1 ± 2	-2 ± 2	-2 ± 1 / -4	-3 ± 4	-8 ± 4	-6 ± -1 / -9	-6 ± 0 / -9	-2 ± 1 / -4	-6 ± -1 / -10
Pilsensee	-8 ± 3	-7 ± 4	-8 ± -3 / -11	-3 ± 3	-2 ± 3	-2 ± 2 / -5	-4 ± 5	-8 ± 6	-8 ± -1 / -12	-8 ± -1 / -11	-3 ± 1 / -5	-6 ± 0 / -11
Nagymohos	-6 ± 2	-6 ± 2	-6 ± -4 / -8	-5 ± 2	-4 ± 2	-3 ± -1 / -5	-1 ± 3	-6 ± 3	-4 ± 0 / -6	-6 ± -2 / -8	-4 ± -2 / -6	-4 ± 0 / -7
Eifel	-6 ± 3	-6 ± 3	-6 ± -2 / -8	-4 ± 2	0 ± 2	0 ± 3 / -2	-1 ± 4	-7 ± 4	-7 ± -1 / -10	-6 ± 0 / -8	-1 ± 2 / -4	-5 ± 1 / -10
La Grotte Walou	-3 ± 4	-5 ± 4	-3 ± 2 / -7	-1 ± 3	0 ± 3	1 ± 6 / -1	-1 ± 5	-7 ± 5	-4 ± 3 / -7	-4 ± 4 / -7	0 ± 4 / -3	-4 ± 2 / -9
Kersdorf-Briesen	-6 ± 4	-5 ± 4	-6 ± -1 / -10	-6 ± 3	-3 ± 4	-4 ± 1 / -6	-4 ± 5	-7 ± 6	-6 ± 1 / -10	-6 ± 2 / -10	-4 ± 0 / -8	-6 ± 1 / -11
Mickunai	-3 ± 5	-1 ± 5	0 ± 6 / -3	-12 ± 4	-2 ± 4	-1 ± 5 / -3	-2 ± 7	-3 ± 8	0 ± 7 / -4	-1 ± 8 / -6	-5 ± 2 / -11	-2 ± 6 / -8
Mean population SD	-8 ± 3	-7 ± 2	-7 ± 2	-6 ± 3	-4 ± 2	-3 ± 2	-4 ± 4	-8 ± 3	-8 ± 4	-7 ± 2	-4 ± 2	-7 ± 3

***Table 3**. Climate anomaly results (°C) for TANN (mean annual temperature), MTWA (mean temperature of the warmest month), and MTCO (mean temperature of the coldest month) from three different methods using the biomization **(a)** and mebiomization **(b)** procedures across 43 pollen sites. In the "Mean multi-method results" column, errors (1σ) represent the combined uncertainty, calculated as the square root of the sum of inter-point variance and mean internal errors. In contrast, in the row "Mean population SD", values represent the mean of population standard deviations (SD), calculated using population variance (N), without internal error propagation.*

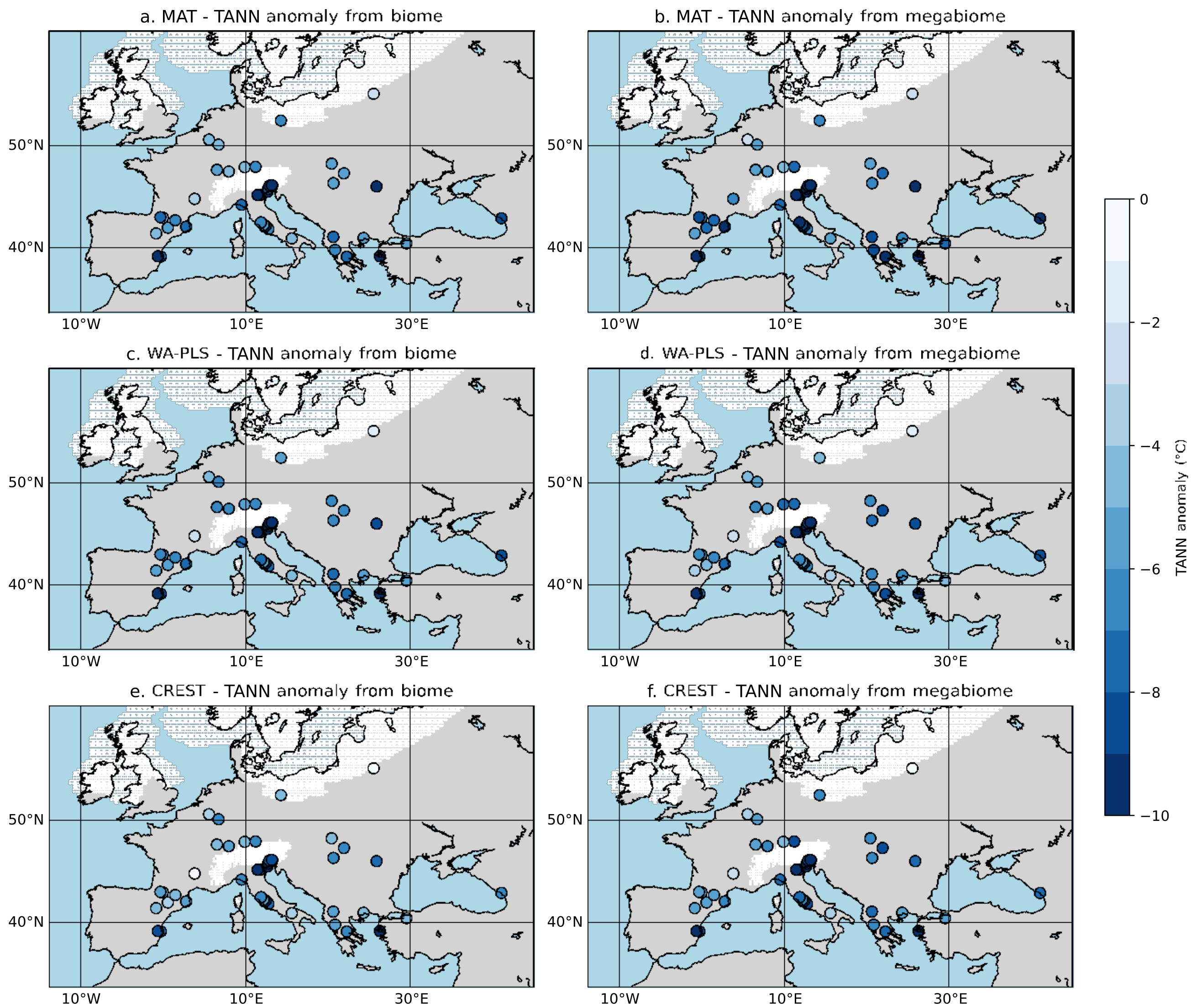

***Figure 6.** Annual temperature anomaly results (LGM – Modern climate) using the biomization **(first line; a, b and c)** and megabiomization **(second line; d, e and f)** processes from three different methods (MAT, WA-PLS and CREST). Modern climates and LGM climate results are reported in **Table 3**. The white area represents the ice sheet extent.*

V.2.3 – Seasonal temperature anomalies

The first row of **Fig.7** (**Figs 7.a-c**) presents reconstructed LGM summer temperature (MTWA) anomalies based on the biomization procedure, with values of −5.8 ± 2.4 °C, −4.3 ± 2.1 °C, and −4.1 ± 2.3 °C (mean SD) for MAT, WA-PLS, and CREST, respectively. The three reconstruction methods yields the most negative MTWA anomalies in southeastern Europe (~−5 °C), whereas values are more homogeneous and closer to zero in northern and western Europe. MTWA anomalies derived from the megabiomization procedure (**Figs 8.a-c**) are −6.1 ± 2.7 °C, −3.7 ± 2.5 °C, and −3.3 ± 2.4 °C for the same reconstruction methods, respectively, yielding similar spatial patterns in MTWA anomalies (**Fig.8**) that from the biome assignments (**Fig.7**). Interestingly, MAT-based MTWA anomalies from the megabiomization procedure (−6.1 ± 2.7 °C) are almost twice as large as those from the WA-PLS and CREST methods (−3.7 ± 2.5 °C, and −3.3 ± 2.4 °C, respectively) for mean values.

The winter temperature (MTCO, second row of **Figs 7 and 8**) anomalies are −6.5 ± 3.5 °C, −8.0 ± 3.2 °C, and −5.6± 3.0 °C from biomization procedure and −4.5 ± 3.8 °C, −9.0 ± 3.5 °C, and −7.8 ± 3.5 °C from megabiomization procedure, for MAT, WA-PLS, and CREST, respectively. MAT-based MTCO anomalies (mean value of -4.5°C) are about half that of CREST (and to a lesser extent WA-PLS) from the megabiomization procedure.

Seasonality anomalies (i.e., seasonal amplitudes) can be calculated from the difference between MTWA and MTCO anomalies at each site, derived from biomization and megabiomization procedures, as shown in the third row of **Figs 7 and 8** (panels g-i). From the biomization procedure (**Fig 7.g-i**), seasonality anomalies (LGM – Modern climate) are generally positive in Western Europe, whereas strongly negative anomalies are mainly observed in Eastern Europe. Results from the megabiomization procedure show seasonality anomaly patterns that differ markedly from those obtained with biomization. Megabiomized anomalies based on WA-PLS and CREST are positive and spatially homogeneous (**Figs 8.h and 8.i**), in contrast to the predominantly negative seasonality anomalies obtained from MAT (**Fig 8.g**). These differences arise from higher MTWA anomalies and lower MTCO anomalies obtained with the MAT method compared to WA-PLS and CREST within the megabiomization procedure. The discrepancies in seasonality anomalies among the three methods under megabiomization are therefore larger than those observed in the standard biomization results.

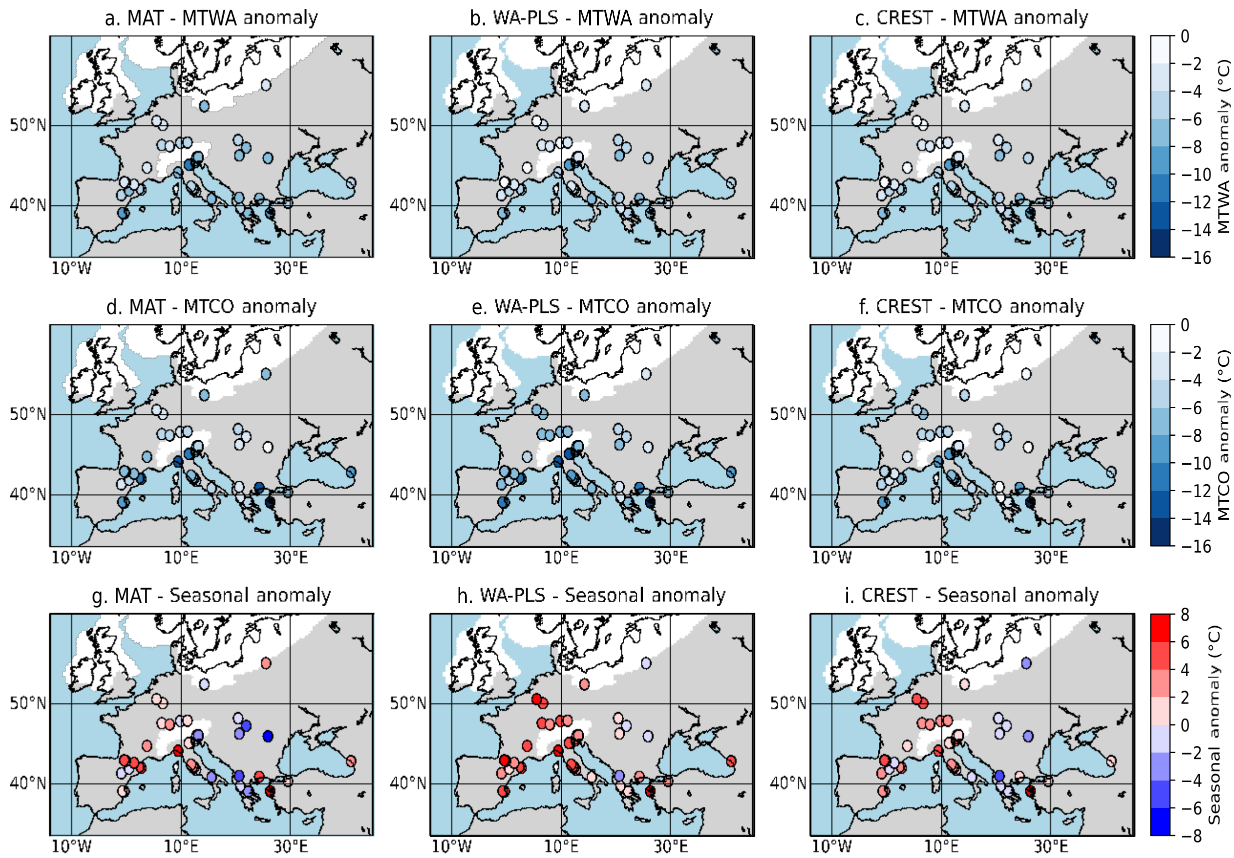

Figure 7. *Monthly (MTWA and MTCO, in **a-c** and **d-f**, respectively) temperature anomaly (LGM – Modern climate) results, using the biomization process for the three different pollen-based climate reconstruction methods. From MTWA and MTCO results, seasonal anomalies are reported on **Figs g-i**. Modern climates and LGM climate results are reported in **Table 3**. The white area represents the ice sheet extent.*

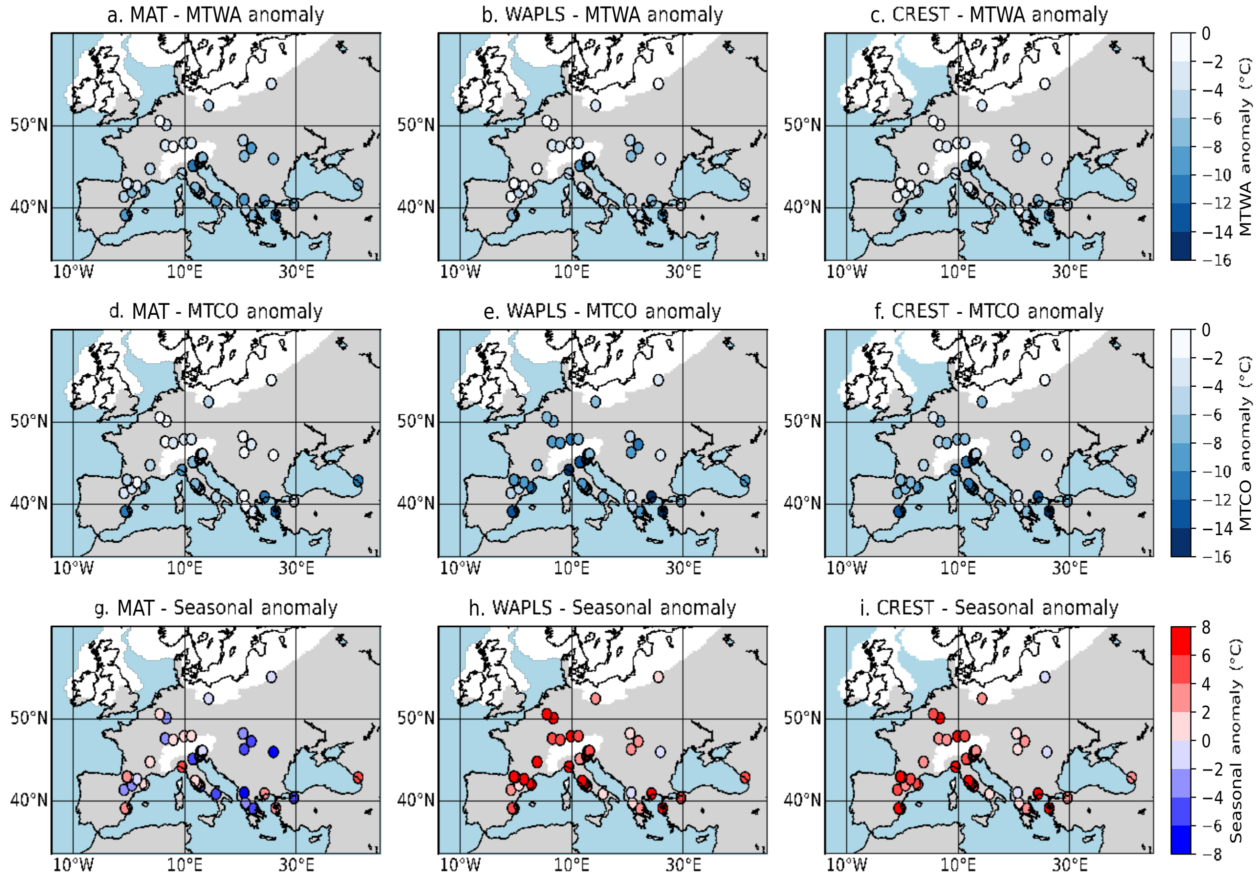

Figure 8. *Monthly (MTWA and MTCO, in **a-c** and **d-f**, respectively) temperature anomaly (LGM – Modern climate) results, using the megabiomization process for the three different pollen-based climate reconstruction methods. From MTWA and MTCO results, seasonal anomalies are reported on **Figs g-i**. Modern climates and LGM climate results are reported in **Table 3**. The white area represents the ice sheet extent.*

V.2.4 - Inter-model means from annual and seasonal temperature anomalies

We summarize in **Fig.9** the arithmetic means of the LGM cooling and seasonality derived from the three approaches, using biomization (**Figs 9.a and 9.c**) and megabiomization (**Figs 9.b and 9.d**) procedures. Mean errors from these two climate variables are reported in **Appendix 6**.

Across Europe, LGM cooling averaged 6.7 ± 2.2 °C and 7.4 ± 2.3 °C (**Table 3**) based on biome and megabiome assignments, respectively (**Fig 9.a-b**). These results are generally consistent across reconstruction methods, with inter-method standard deviations below +2 °C (**Appendix 6**). Inter-model mean MTWA anomalies are similar for both reconstruction methods and for biome versus megabiome assignments, with mean multi-method values of –4.7 ± 2.2 °C and –4.4 ± 2.3 °C, respectively. Inter-model mean MTCO anomalies are –6.7 ± 3.0 °C for the biomization approach (**Fig 7.d–f**) and –7.1 ± 3.4 °C for the megabiomization approach (**Fig 8.d–f**). Mean seasonal anomalies across methods are +2.0 ± 2.5 °C and +2.7 ± 2.7 °C for biome and megabiome assignments, respectively (**Fig 9.c-d**). MAT-based seasonal anomalies are lower (–1.7 ± 3.5°C) than those from WA-PLS and CREST (+5.7 ± 2.8 °C and +3.0 ± 1.3 °C, respectively) using megabiome procedures. In contrast, seasonal anomalies are relatively consistent across methods using the biomization approach, with inter-method standard deviations of ≈ 2°C (**Appendix 6**).

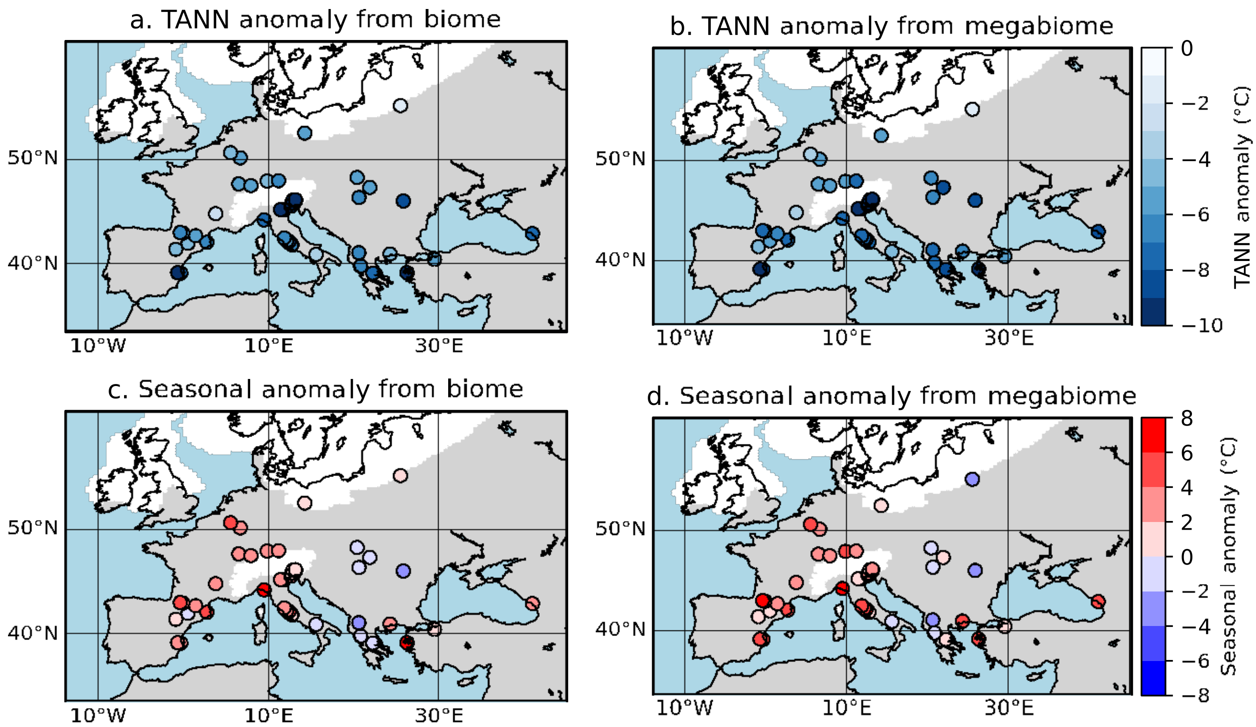

Figure 9. *Mean annual temperature **(a and c)** and seasonal index **(b and d)** anomaly results (LGM – Modern climate) using averages of biomization and megabiomization results from three different pollen-based climate reconstruction methods. Seasonal anomalies = MTWA - MTCO anomalies. Standard deviation maps of climate anomalies are reported in **Appendix 6**. The white area represents the ice sheet extent.*

V.3 – Methodological implications on paleoclimate reconstructions

V.3.1 - Local and global calibration effects on climate reconstructions

To isolate and quantify the impact of local calibration (i.e., (mega)biome procedures) on global climate reconstructions during the LGM across Europe, **Fig 10.a** shows TANN anomalies calculated as the difference between climates obtained using the (mega)biome mean-weighting approaches and those derived from global calibration (i.e., by sampling the entire calibration EMPD2 pollen dataset).

As the MAT method is inherently based on dissimilarity coefficients (*Guiot et al., 1989*), it is theoretically able to directly identify the dominant analogues with no requirement for (mega)biome calibration using all modern pollen spectra. As a result, one expects only a minimal (if any) effect of (mega)biomization on TANN reconstructions from the MAT method (**Fig 10.a**). Here, only a few fossil sites show a warming effect (~+5°C) of reconstructed TANN using local calibrations based on (mega)biomes (Venice, Billerio and Feher) rather than the global calibration. Then, the MAT method is thus arguably suitable for large-scale spatial studies using global datasets, to reconstruct annual temperature across Europe. Although the effects of local versus global calibration TANN anomalies for MAT may depend on the time period considered and the reconstructed climate variables (*Xu et al., 2010*), the magnitude of these effects remain generally close to zero. However, the WA-PLS method produces generally inconsistent results between local and global calibration results, with a mean TANN anomaly of ~-4.5°C, indicating colder TANN using local rather than global calibrations. Two significantly negative anomalies (~-10°C), were also identified using the WA-PLS method (Lake Iznik, Kersdorf-Briesen). Similarly, the CREST method appears more sensitive to calibration, as evidenced by predominantly negative TANN anomalies (from -1.2°C to -10.9°C, with a mean of -6.5°C, **Fig 10.a**). This underscores the importance of a robust (mega)biomization scheme – climatic and environmental gradients of the study area – when applying CREST in Europe during the LGM to ensure that reconstructed TANN remains sufficiently cold and consistent with other statistical methods (see **Figs 6 and 9**). The importance of modern regional calibrations for quantitative climate reconstructions has also been noticed in previous studies (e.g., *Trasune et al., 2024*).

In **Fig 10.b**, the application of the (mega)biomization methods to MAT, WA-PLS and CREST does not significantly impact the reconstructed MTWA (~0°C on average from the difference between local and global calibration). In **Fig 10.c**, the differences in MTCO anomaly results between local and global calibrations are however more variable than MTWA results, across fossil sites. In detail, the MAT method generally produces larger MTCO anomalies with local calibration than with global calibration (+4.0°C on average), whereas the WA-PLS and CREST methods tend to yield similarly lower MTCO anomalies (−4.5°C on average). These findings highlight an opposite effect of the (mega)biomization procedure from the MAT versus WA-PLS and CREST methods in reconstructing the MTCO variable.

For TANN and MTWA reconstructions, MAT appears to be the most suitable reconstruction method, for identifying dominant analogues within a global calibration dataset to infer past climate conditions. However, MTCO outputs are sensitive to the modern subsamples defined by biome and megabiome classifications (**Fig.10**), from MAT and CREST methods.

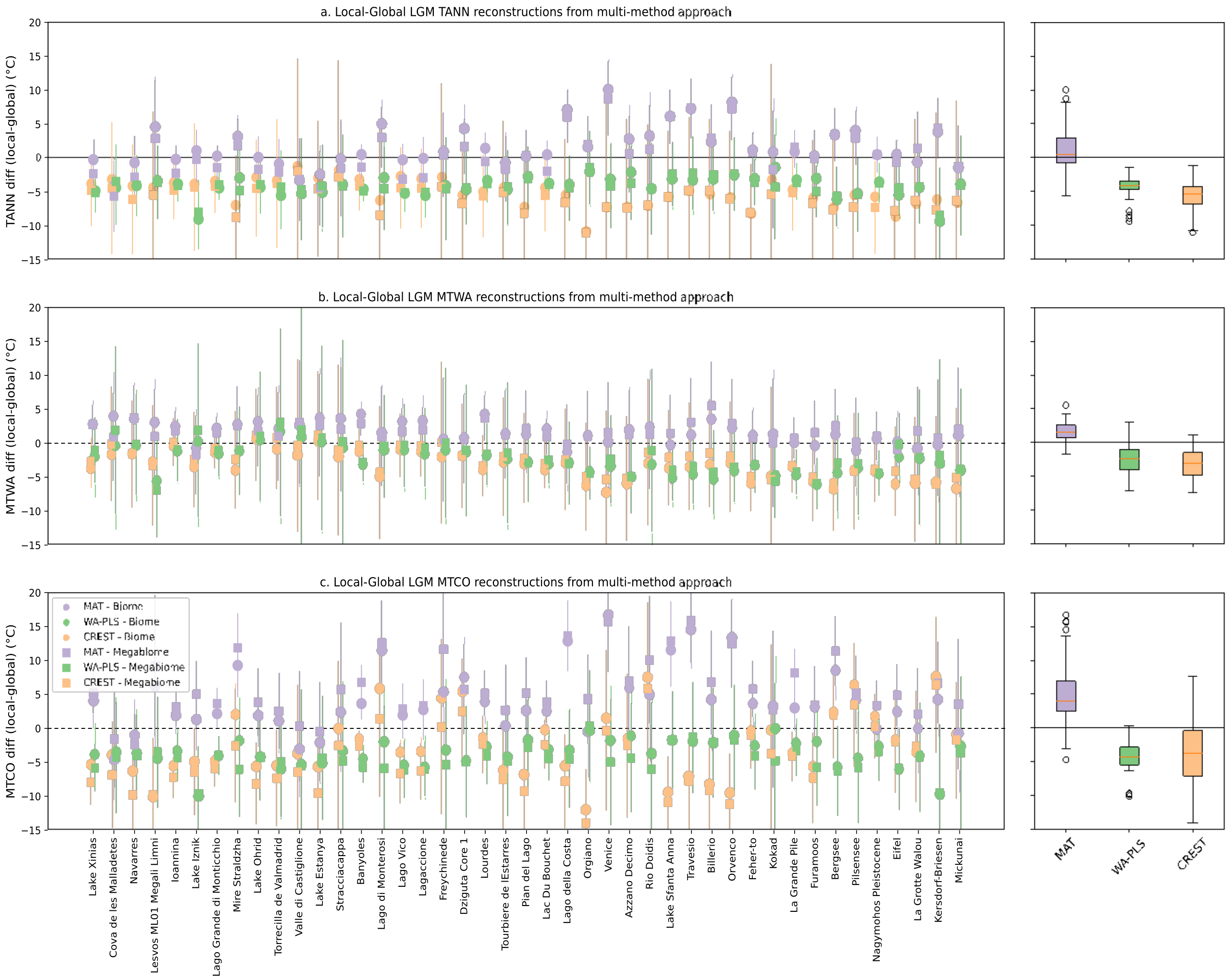

Figure 10. *Mean LGM annual temperature* ***(a)****, MTWA* ***(b)*** *and MTCO* ***(c)*** *anomalies for each fossil site, calculated as the difference between (mega)biomized and not-(mega)biomized (global calibration) climate variables for the three methods of pollen-based climate reconstruction. The biomization and megabiomization results are shown using circle and square symbols, respectively. Site names are arranged (left to right) in ascending order of latitude. Results are reported* ***Table 3.*** *Errors are 1σ. The boxplots on the right represent the distributions of the mean local–global differences for each climate variable across reconstruction methods (in color).*

V.3.2 - Biomization vs. Megabiomization effects on climate reconstructions

Across reconstruction methods, TANN and MTWA results derived from the biomization process are consistent with the megabiomization outputs (i.e., anomalies defined as the difference between the two treatments - are close to 0, **Figs 11.a and 11.b**). This result highlights the minimal impact of distinguishing between cold and hot arid conditions into steppe and desert biomes (not the case for megabiomes) on reconstructed LGM TANN and MTWA in Europe from three different methods.

However, MTCO anomaly results from MAT show slightly lower anomalies, by a few degrees (-2.5°C on average, **Fig 11.c**), when using biomes instead of megabiomes, suggesting a further flattening of seasonal amplitude compared to present-day conditions (see **Fig 8-9**). While the differences in MTCO obtained by WA-PLS between biome and megabiome classifications vary across sites, biome-based MTCO anomaly results from CREST generally show greater anomalies than those obtained using the megabiome procedure (~+2°C on average, **Fig 11.c**).

In summary, MAT-based biomization increases seasonality at some sites compared to the megabiomization process, which can be explained by MTCO anomalies being lower using biomization compared to megabiomization (–6.5°C vs. –4.5°C on average). CREST methods also show a high sensitivity to local calibrations, with higher MTCO anomalies from biomes compared to megabiomes (-5.7°C vs. –7.8°C on average). MAT and CREST methods exhibit a strong dependence on the calibration dataset for winter temperature reconstructions, which could be attributed to the spatial variability of MTCO anomalies in the modern calibration dataset. Overall, these results highlight the dependence of climate reconstructions on the chosen method, calibration, and climatic variables.

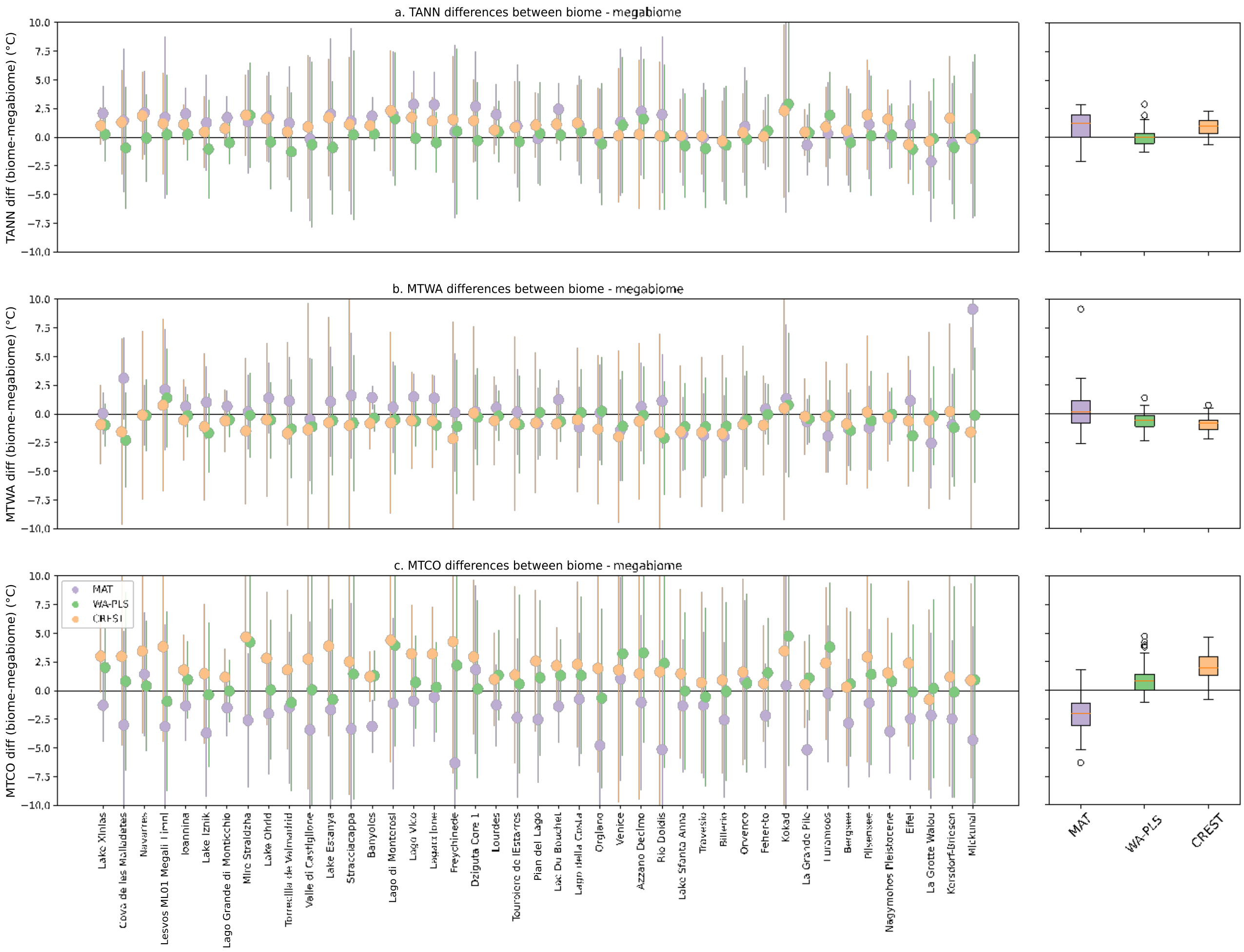

Figure 11. *Mean LGM annual temperature **(a)**, MTWA **(b)** and MTCO **(c)** anomalies for each fossil site, calculated as the difference between biomized and megabiomized climate variables for the three methods of pollen-based climate reconstruction. Site names are arranged in ascending order of latitude. Results are reported **Table 3**. Errors are 1σ. The*

boxplots on the right represent the distributions of the mean biome–megabiome differences for each climate variable across reconstruction methods (in color).

VI. <u>Discussion</u>

VI.1 - Comparing vegetation distributions from the (mega)biome assignments

The pollen-based modern biome distribution (**Fig.2**) closely resembles European results obtained using the same biomization method as *Prentice et al. (1998)*. In particular, the diversity of biomes in Spain (TEDE, COMX, XERO, and WAST), as well as the geographic extent of temperate forests and xerophytic vegetation, aligns well with previous findings (*Hengl et al., 2018*). However, our results indicate a broader modern extent of cold forest (CLMX) across the Scandinavian countries, relative to *Prentice et al. (1998)*.

In 2017, *Binney et al.* proposed a BIOME 6000 approach, building upon *Prentice and Webb III (1998)*, to identify dominant biomes using the biomization procedure of *Bigelow et al. (2003)*, super-PFT contributions, and BIOME 4 model biomes (*Kaplan et al., 2003*). Their biome distributions similarly reveal patterns for the TEDE, TAIGA, and TUND biomes, although with a stronger TUND dominance in Northern Europe compared to our results. Meanwhile, during the LGM, *Kaplan et al. (2016)* show that forest-cover reconstructions from vegetation models constrained by climate simulations suggest greater forest cover - and consequently less extensive steppe conditions - than pollen-based reconstructions indicate.

Furthermore, the “Regional Estimates of Vegetation Abundance from Large Sites” (REVEALS) land-cover model, described by *Kern et al. (2024)*, compiles European pollen datasets to reconstruct plant-specific parameters over time, including high-frequency events. A comparison between outputs from this vegetation model and LGM megabiome results indicates an overrepresentation of modeled arboreal vegetation (**Fig. 2**), at the expense of grasses and herbs. This discrepancy may reflect an aridification bias in climate reconstructions based on the megabiome approach.

Global megabiome reconstructions in this study closely match modeled vegetation distributions from *Li et al. (2025)* and align with previous European results using the same biomization procedure (*Bigelow et al., 2003*), demonstrating good reproducibility across Europe.

Then, the modern (mega)biome distribution is geographically coherent, seemingly realistic and compatible with previous studies, thus confirming the robustness of our biome outputs for European climate reconstructions.

VI.2 - Comparing climate reconstructions

As shown in **Figs 6 and 9**, the climate reconstruction methods (MAT, WA-PLS, and CREST) using (mega)biomization procedures globally yield similar results, as indicated by the high correlation coefficients ($R^2 \geq 71\%$, **Figs 12.a-f**) across reconstruction methods. The significance of the regressions (R^2) is maintained between the biomization and megabiomization approaches, although TANN reconstructions derived from CREST are somewhat less consistent with MAT under the megabiomization procedure compared to the biomization approach (R^2=82% and 84%, from biome and megabiome techniques, respectively, **Fig 12.a-b**). Moreover, the climates inferred from CREST appear to be more closely correlated with WA-PLS than with MAT results, with R^2 values systematically higher for "CREST vs. WA-PLS" than for "CREST vs. MAT" in **Fig 12.**

A key advantage of this multi-method approach is that it isolates the intrinsic properties, behaviors, and weaknesses of each method. While MAT is highly dependent on the quality of analogues (*Chevalier et al., 2020*), it performs well for pollen taxa with low taxonomic resolution (at the family and genus level). WA-PLS is also sensitive to the choice of modern dataset (e.g., situations with low analogue availability, *Birks and Seppä, 2010*), and it relies on unimodal vegetation-climate response (*Ter Braak and Juggins, 1993*). CREST method is less effective for taxa with low taxonomic resolution, accounts for multimodal vegetation responses to climate (*Chevalier et al., 2014*). However, because TANN, MTWA and MTCO exhibit homogeneous patterns across Europe and spatial averages of the three methods yield comparable results, we can average outputs (mean SD) from the three reconstruction methods to provide spatial mean climate variables during the LGM: –6.7±2.1 °C in TANN anomalies, –4.8±2.2 °C in MTWA anomalies, and –6.7±3.0 °C MTCO anomalies from biomization procedure, and –7.4 ±2.3 °C in TANN anomalies, –4.4±2.3°C in MTWA anomalies, and –7.1±3.4 °C MTCO anomalies from megabiomization procedure across Europe. Thus, despite using the same modern and fossil datasets, these methods yield distinct but complementary LGM climate reconstructions that can be combined together to provide robust estimates for the reconstructed climate variables.

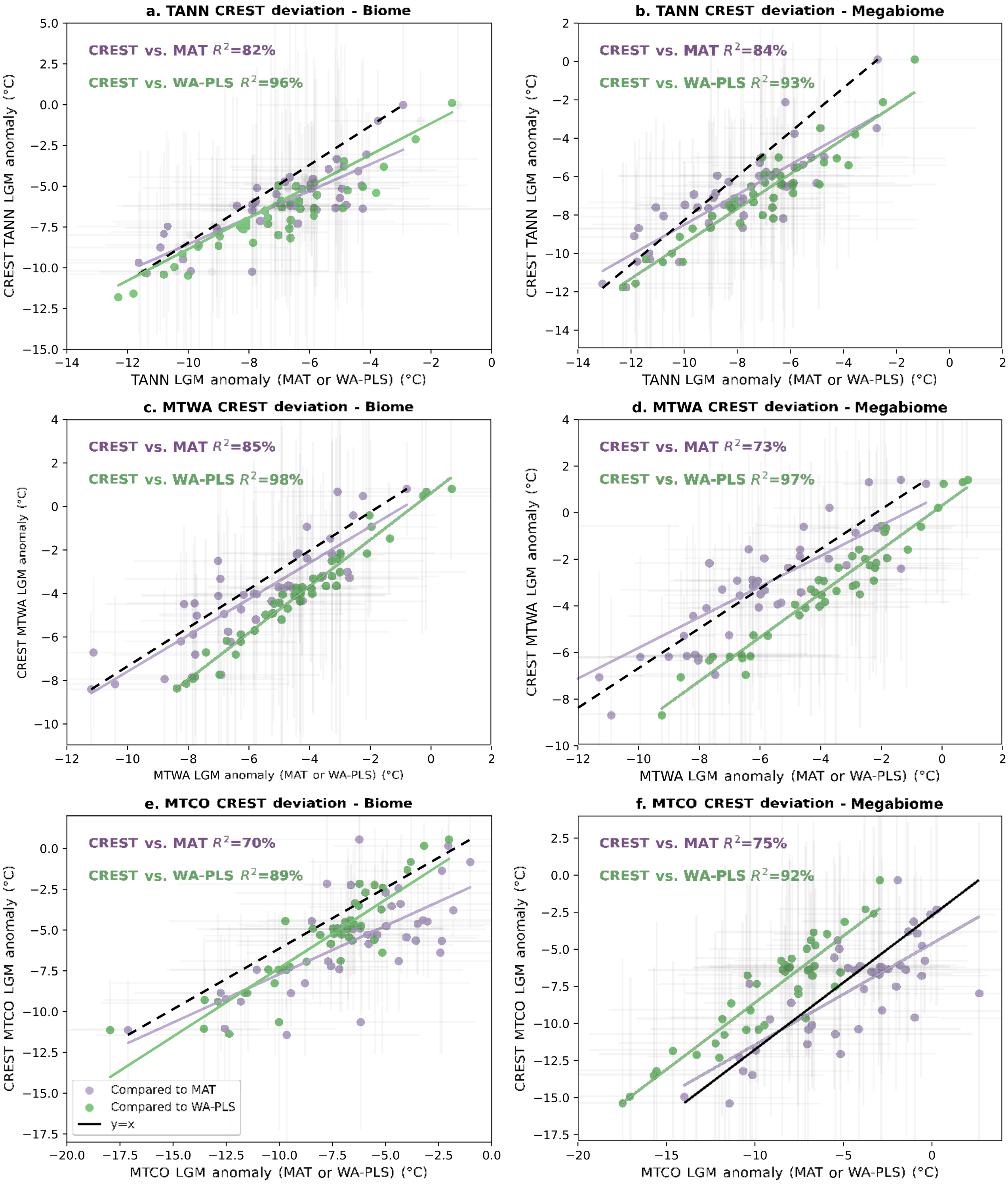

Figure 12. *Linear relationship between TANN* ***(a and b)****, MTWA* ***(c and d)*** *and MTCO* ***(e and f)*** *anomaly results (LGM – Modern climate) from the three pollen-based climate reconstruction methods, using biomization and megabiomization procedures. All R^2 values reported in this study are statistically significant, with p values < 0.01. These plots show relationships between CREST results and those from statistical methods (MAT in blue and WA-PLS in green) from the 43 fossil sites. Errors are 1σ.*

VI.3 – Pollen-based reconstruction comparisons from literature

VI.3.1 - Local calibration effects from MAT-based climate reconstructions: comparison with *Davis et al. (2024)*

To study the reliability of our LGM climate reconstructions with results published in literature, we compare our biomized and megabiomized multi-method results for three different climate variables with those of *Davis et al. 2024. Davis et al. 2024* also used the calibration dataset (EMPD2 dataset) and some input fossil records, common with our study. Comparison maps (differences) between the two studies are presented in **Appendix 7** and summarized as boxplots in **Fig.13**. We use error metrics to compare the results of the two studies and assess the effect of methodological differences on climate reconstructions. Unlike R^2, which is insensitive to systematic biases, error metrics (RMSE) express deviations in the original units (°C), making them more suitable for comparison.

The TANN and MTWA errors (RMSE) between our multi-method reconstructions and those of *Davis et al. (2024)* are comparable to the individual reconstruction errors (2–3°C; **Figs. 13a–b**), indicating relatively good agreement between the studies regardless of the calibration ((mega)biomization) and reconstruction methods. In contrast, MTCO anomalies show larger discrepancies between the two studies (4–5°C; **Fig. 13c**). MTCO results exhibit poorer agreement between the two studies, with RMSE values approximately twice as high as those for TANN and MTWA (**Fig. 13c**), particularly for megabiomization (~4.9°C) compared to biomization (~4.3°C). Overall, across these three methods, the results of *Davis et al. (2024)* agree more closely with our biomization-based reconstructions than with those based on megabiomization, with RMSE differences ranging from 0.5 to 1.5°C. From **Appendix 7**, our study also shows that climatic conditions at sites located closest to the Fennoscandian ice sheet are systematically warmer (+5°C to +10°C) in our study compared to *Davis et al. (2024)*. Interestingly, our approach leads to substantially higher MTCO anomalies in Northern Europe (~+3°C) and lower MTCO anomalies in Southern Europe (~−3°C).

These results align with those reported in ***section V.3***, highlighting the predominant influence of the (mega)biome-type assignment scheme (**Figs 10.c** and **11.b**) and reconstruction methods on MTCO anomalies, likely due to the high spatial variability of modern data within the calibration dataset. MTCO reconstructions show the strongest inter-study inconsistencies and are particularly sensitive to methodological choices. The difference in modern calibration samples used in *Davis et al. 2024* and in the (mega)biome definitions of our study may explain the observed differences in reconstructed temperature, particularly the large MTCO discrepancies. These discrepancies demonstrate the strong methodological dependence of palaeoclimate reconstructions and the importance of systematic cross-validation frameworks.

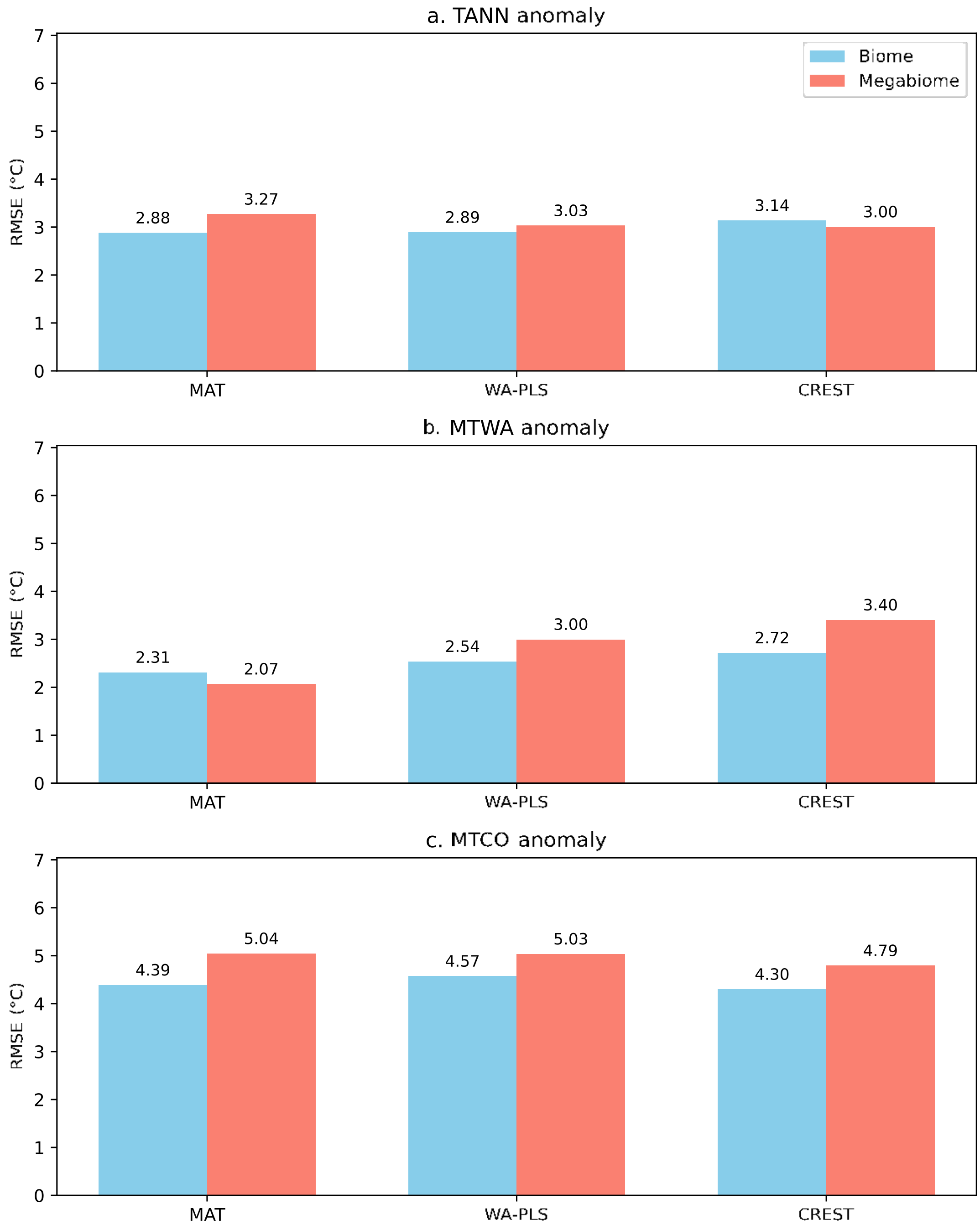

Figure 13. *RMSE of mean annual* ***(a)*** *and monthly anomalies* ***(b and c)*** *(LGM – Modern climate) between our three reconstruction methods (MAT, WA-PLS, CREST) and results from Davis et al. (2024). Bars represent RMSE for Biome (blue) and Megabiome (orange), with RMSE values reported above each bar to indicate the reconstruction error relative to Davis et al. (2024).*

VI.3.2 - Systematic climate discrepancies between pollen data and models

The extent of LGM cooling inferred in this study ranges from 0°C to −10°C relative to present (**Fig.6**) and appears to fall within the range simulated by climate models (e.g., *Kageyama et al., 2021*). We also provide new constraints on LGM temperature seasonality indicating an amplification near the Atlantic coasts and a relative reduction inland, compared to present day. This continental pattern of LGM seasonality is in strong agreement with the mean model from PMIP synthesis by *Izumi et al. (2013)*, which shows a gradient from positive anomalies in Spain (+10°C) to negative anomalies (–4°C) in Eastern Europe.

However, comparing pollen-based climate reconstructions with climate model outputs is complex due to both the heterogeneous spatial coverage of the data, the variability of reconstruction methods and the dispersion among climate models (e.g., *Bartlein et al., 2011; Kageyama et al., 2021*). Moreover, proxies record extreme and local climates, while climate models tend to provide spatially-averaged climate conditions. Ongoing improvements in the spatial resolution of regional climate models make comparisons with local proxies increasingly appropriate, although significant data–model discrepancies remain (*Kageyama et al., 2021*). Similarly, expanding the availability of pollen data in Europe would further improve the robustness of such comparisons.

VII. Conclusion

This study presents the first comprehensive comparison of pollen-based climate reconstruction methods applied to the LGM in Europe, using a local calibration framework integrating both biomization and megabiomization techniques. The approach is applied to a compilation of fossil sites spanning the LGM and compared against a comprehensive modern calibration dataset (EMPD2). We propose a new conservative method for weighting reconstructed climate variables from (mega)biome affinity scores, which corrects for threshold effects in (mega)biome shifts and incorporates their continuous variations over time. We isolate and quantify the effects of calibration, biome score application methods, and reconstruction techniques on the inferred paleoclimates, and synthesize them in the form of inter-model means and deviations.

In Europe, the TANN anomalies (mean SD) obtained with biomization are –7.0±2.3°C (MAT), –7.1±2.2°C (WA-PLS), and –5.9 ±2.2°C (CREST), whereas those derived from megabiomization are –8.0±2.5°C (MAT), –7.2±2.4°C (WA-PLS), and –7.0±2.3°C (CREST). Due to these consistent results, we propose LGM climate anomalies (from climate modern) based on a mean model integrating the three reconstruction methods: –6.7±2.1°C in TANN anomalies, –4.8±2.2 °C in MTWA anomalies, and –6.7±3.0°C MTCO anomalies from biomization procedure, and –7.4 ±2.3°C in TANN anomalies, –4.4±2.3°C in MTWA anomalies, and –7.1±3.4 °C MTCO anomalies from megabiomization procedure across Europe.

The dependence of reconstruction method outputs on (mega)biome calibrations vary depending on both the climate variables and the fossil pollen assemblages (i.e., the sites). Local calibration is necessary for WA-PLS and CREST-based reconstructions due to the underrepresentation of cold climates in Europe. These results show that, using the biome and megabiome calibrations, the CREST (probabilistic) method shows LGM climate results generally consistent with those of statistical approaches (MAT and WA-PLS), although the consistency of CREST and WA-PLS reconstructions is slightly better than with MAT. Winter temperature (MTCO) results exhibit higher sensitivity to reconstruction methods and (mega)biomization approaches than TANN and MTWA results. Based on MTCO reconstructions, the WA-PLS and CREST method shows an opposite response to local calibration compared with MAT, amplifying seasonal anomalies relative to global calibration (+4.5°C for CREST and -4°C for MAT on average) while reducing European LGM seasonality by the biomization procedure, but less strongly (-2.5°C for CREST and +2°C for MAT on average).

Scientific contributions - Authorship contribution statement

Role of each author: Fénisse G. wrote the original draft of the manuscript, which was reviewed and edited by all co-authors.

Acknowledgements

This study is financially supported by the ANR (ANR-22-CPJ2-0005-24/39 584 01, awarded to D.V. Bekaert). Manuel Chevalier was supported by the German Federal Ministry of Education and Research (BMBF) as a Research for Sustainability initiative (FONA; https://www.fona.de/en/) through the PalMod Phase II and Phase III projects (grant no. 01LP1926D and 01LP2308B).

Appendix

Our results including (i) compilation maps from fossil and modern pollen data; (ii) observed vs. Predicted relationship; (iii) monthly climate reconstructions since the LGM and (iv) standard deviation of four climate variables are available in the online open repository ORDAR:

https://doi.org/10.24396/ORDAR-231

Code and data availability

All support data including (i) the exhaustive modern datasets and fossil pollen samples derived from the literature; (ii) our training code of (mega-)biome and three reconstruction methods; and (iii) our climate results are available in the online open repository ORDAR:

https://doi.org/10.24396/ORDAR-232

List of Appendix

1. Site location, type of archives (a) and pollen description using taxonomic diversity parameters (b) and AP/NAP percentages (c) in 43 pollen LGM records.
2. Relationship between biome and megabiome
3. Pollen taxa observed from the fossil pollen cores

4. Percentage of arid megabiomes (STEP+DESE+TUND) at the LGM in 43 pollen sequences. Red contour points referred to the TEDE dominant megabiomes. SAVA scores are negligible.
5. Cross validation procedures between observed and predicted modern climate variables of the pollen datasets (EMPD2 dataset).
6. Standard deviation of annual temperature (a), precipitation (b), MTWA (c) and MTCO (d) anomaly results (LGM – Modern climate) using averages of biomization results from 3 different methods.
7. Mean annual and monthly map anomalies reconstructed using three methods based on biomization and megabiomization, compared with Davis et al. (2024).

References

Arslanov, K. A., Dolukhanov, P. M., and Gei, N. A.: Climate, Black Sea levels and human settlements in Caucasus Littoral 50,000–9000 BP, Quatern. Int., 167–168, 121–127, https://doi.org/10.1016/j.quaint.2007.02.013, 2007.

Bartlein, P.J., Harrison, S.P., Brewer, S., Connor, S., Davis, B.A.S., Gajewski, K., Guiot, J., Harrison-Prentice, T.I., Henderson, A., Peyron, O., Prentice, I.C., Scholze, M., Seppä, H., Shuman, B., Sugita, S., Thompson, R.S., Viau, A.E., Williams, J., Wu, H.: Pollen-based continental climate reconstructions at 6 and 21 ka: a global synthesis. Clim. Dyn. 37, 775–802. https://doi.org/10.1007/s00382-010-0904-1, 2011.

Bigelow, N.H., Brubaker, L.B., Edwards, M.E., Harrison, S.P., Prentice, I.C., Anderson, P.M., Andreev, A.A., Bartlein, P.J., Christensen, T.R., Cramer, W., Kaplan, J.O., Lozhkin, A.V., Matveyeva, N.V., Murray, D.F., McGuire, A.D., Razzhivin, V.Y., Ritchie, J.C., Smith, B., Walker, D.A., Gajewski, K., Wolf, V., Holmqvist, B.H., Igarashi, Y., Kremenetskii, K., Paus, A., Pisaric, M.F.J., Volkova, V.S.: Climate change and Arctic ecosystems: 1. Vegetation changes north of 55°N between the last glacial maximum, mid-Holocene, and present. J. Geophys. Res. Atmospheres 108, 2002JD002558. https://doi.org/10.1029/2002JD002558, 2003.

Binney, H., Edwards, M., Macias-Fauria, M., Lozhkin, A., Anderson, P., Kaplan, J.O., Andreev, A., Bezrukova, E., Blyakharchuk, T., Jankovska, V., Khazina, I., Krivonogov, S., Kremenetski, K., Nield, J., Novenko, E., Ryabogina, N., Solovieva, N., Willis, K., Zernitskaya, V.: Vegetation of Eurasia from the last glacial maximum to present: Key biogeographic patterns. Quat. Sci. Rev. 157, 80–97. https://doi.org/10.1016/j.quascirev.2016.11.022, 2017.

Birks, H.J.B.: Quantitative palaeoenvironmental reconstructions. Stat Model Quat Sci Data Tech Guid., Statistical Modelling of Quaternary Science Data., Technical Guide 5, Quaternary Research Association, Cambridge. 271 pp., 1995.

Birks, H.J.B., Seppä, H.: Pollen-based reconstructions of late-Quaternary climate in Europe – progress, problems, and pitfalls., Acta Palaeobotanica 44(2): 317–334, 2004

Blaauw, M., Wohlfarth, B., Christen, J.A., Ampel, L., Veres, D., Hughen, K.A., Preusser, F., Svensson, A.: Were last glacial climate events simultaneous between Greenland and France? A quantitative comparison using non-tuned chronologies. J. Quat. Sci. 25, 387–394. https://doi.org/10.1002/jqs.1330, 2010.

Bonatti, E.: Pollen sequence in the lake sediments. In: Hutchinson, G. E. (ed.), Lanula: an Account of the History and Development of the Lago di Monterosi, Latium, Italy, T. Am. Philos. Soc., 60, 26–31, https://doi.org/10.2307/1005996, 1970.

Bottema, S.: Pollen analytical investigations in Thessaly (Greece), Palaeohistoria, 21, 19–40, 1979.

Braconnot, P., Harrison, S.P., Kageyama, M., Bartlein, P.J., Masson-Delmotte, V., Abe-Ouchi, A., Otto-Bliesner, B., Zhao, Y.: Evaluation of climate models using palaeoclimatic data. Nat. Clim. Change 2, 417–424. https://doi.org/10.1038/nclimate1456, 2012.

Brewer, S., Guiot, J., Sánchez-Goñi, M.F., Klotz, S.: The climate in Europe during the Eemian: a multi-method approach using pollen data. Quat. Sci. Rev. 27, 2303–2315. https://doi.org/10.1016/j.quascirev.2008.08.029, 2008.

Cao, X., Herzschuh, U., Telford, R.J., Ni, J.: A modern pollen–climate dataset from China and Mongolia: Assessing its potential for climate reconstruction. Rev. Palaeobot. Palynol. 211, 87–96. https://doi.org/10.1016/j.revpalbo.2014.08.007, 2014.

Cao, X., Tian, F.: Pollen-based biome reconstruction in R. Zenodo Code. https://doi.org/10.5281/zenodo.7523423, 2021.

Cao, X., Tian, F., Dallmeyer, A., Herzschuh, U.: Northern Hemisphere biome changes (>30°N) since 40 cal ka BP and their driving factors inferred from model-data comparisons. Quat. Sci. Rev. 220, 291–309. https://doi.org/10.1016/j.quascirev.2019.07.034, 2019.

Cao, X., Tian, F., Herzschuh, U., Ni, J., Xu, Q., Li, W., Zhang, Y., Luo, M., Chen, F.: Human activities have reduced plant diversity in eastern China over the last two millennia. Glob. Change Biol. 28, 4962–4976. https://doi.org/10.1111/gcb.16274, 2022.

Carrión, J. S. and Dupré-Olivier, M.: Late Quaternary vegetational history of Navarrés, eastern Spain. A two core approach, New Phytol., 134, 177–191, https://doi.org/10.1111/j.14698137.1996.tb01157.x, 1996.

Charton, L., Combourieu-Nebout, N., Bertini, A., Lebreton, V., Peyron, O., Robles, M., Sassoon, D., Moncel, M.-H. : Vegetation and climate changes during the Middle to Upper Palaeolithic transition in the southwestern Mediterranean: What happened to the last Neanderthals during Heinrich stadial 4? Quat. Sci. Rev. 359, 109345. https://doi.org/10.1016/j.quascirev.2025.109345, 2025.

Chevalier, M.: *crestr* : an R package to perform probabilistic climate reconstructions from palaeoecological datasets. Clim. Past 18, 821–844. https://doi.org/10.5194/cp-18-821-2022, 2022.

Chevalier, M., Davis, B.A.S., Heiri, O., Seppä, H., Chase, B.M., Gajewski, K., Lacourse, T., Telford, R.J., Finsinger, W., Guiot, J., Kühl, N., Maezumi, S.Y., Tipton, J.R., Carter, V.A., Brussel, T., Phelps, L.N., Dawson, A., Zanon, M., Vallé, F., Nolan, C., Mauri, A., De Vernal, A., Izumi, K., Holmström, L., Marsicek, J., Goring, S., Sommer, P.S., Chaput, M., Kupriyanov, D.: Pollen-based climate reconstruction techniques for late Quaternary studies. Earth-Sci. Rev. 210, 103384. https://doi.org/10.1016/j.earscirev.2020.103384, 2020.

Chevalier, M.: Enabling possibilities to quantify past climate from fossil assemblages at a global scale. Glob. Planet. Change 175, 27–35. https://doi.org/10.1016/j.gloplacha.2019.01.016, 2019.

Chevalier, M., Chase, B.M.: Determining the drivers of long-term aridity variability: a southern African case study. J. Quat. Sci. 31, 143–151. https://doi.org/10.1002/jqs.2850, 2016.

Chevalier, M., Chase, B.M.: Southeast African records reveal a coherent shift from high- to low-latitude forcing mechanisms along the east African margin across last glacial–interglacial transition. Quat. Sci. Rev. 125, 117–130. https://doi.org/10.1016/j.quascirev.2015.07.009, 2015.

Chevalier, M., Chase, B.M., Quick, L.J., Dupont, L.M., Johnson, T.C.: Temperature change in subtropical southeastern Africa during the past 790,000 yr. Geology 49, 71–75. https://doi.org/10.1130/G47841.1, 2021.

Chevalier, M., Cheddadi, R., Chase, B.M.: CREST (Climate REconstruction SofTware): a probability density function (PDF)-based quantitative climate reconstruction method. Clim. Past 10, 2081–2098. https://doi.org/10.5194/cp-10-2081-2014, 2014.

Chevalier, M., Davis, B.A.S., Heiri, O., Seppä, H., Chase, B.M., Gajewski, K., Lacourse, T., Telford, R.J., Finsinger, W., Guiot, J., Kühl, N., Maezumi, S.Y., Tipton, J.R., Carter, V.A., Brussel, T., Phelps, L.N., Dawson, A., Zanon, M., Vallé, F., Nolan, C., Mauri, A., De Vernal, A., Izumi, K., Holmström, L., Marsicek, J., Goring, S., Sommer, P.S., Chaput, M., Kupriyanov, D.: Pollen-based climate reconstruction techniques for late Quaternary studies. Earth-Sci. Rev. 210, 103384. https://doi.org/10.1016/j.earscirev.2020.103384, 2020.

Cleator, S.F., Harrison, S.P., Nichols, N.K., Prentice, I.C., Roulstone, I.: A new multivariable benchmark for Last Glacial Maximum climate simulations. Clim Past., 16, 699–712, https://doi.org/10.5194/cp-16-699-2020, 2020

Cruz-Silva, E., Harrison, S.P., Marinova, E., Prentice, I.C.: A new method based on surface-sample pollen data for reconstructing palaeovegetation patterns. J. Biogeogr. 49, 1381–1396. https://doi.org/10.1111/jbi.14448, 2022.

Dallmeyer, A., Claussen, M., Brovkin, V.: Harmonising plant functional type distributions for evaluating Earth system models. Clim. Past 15, 335–366. https://doi.org/10.5194/cp-15-335-2019, 2019.

Damblon, F. : L'enregistrement palynologique de la sequence pléistocène et holocène de la grotte Walou, in: La grotte Walou à Trooz (Belgique), edited by: Draily, C., Pirson, S., and Toussaint, M., Service public de Wallonie (Etudes et Documents, Archéologie, 21), https://www.academia.edu/23006376/Draily_C_Toussaint_M_and_Pirson_S_Dir_2011_La_grotte_Walou_%E0_Trooz_Belgique_Fouilles_de_1996_%E0_2004_Volume_2_Les_sciences_de_la_vie_et_les_datations_Monographie_Etudes_et_documents_Arch%E9ologie_21_Namur_Service_public_de_Wallonie_241_p (last access: 25 July 2024), 84–129, 2011.

Daniau, A.-L., Desprat, S., Aleman, J.C., Bremond, L., Davis, B., Fletcher, W., Marlon, J.R., Marquer, L., Montade, V., Morales-Molino, C., Naughton, F., Rius, D., Urrego, D.H.: Terrestrial plant microfossils in palaeoenvironmental studies, pollen, microcharcoal and phytolith. Towards a comprehensive understanding of vegetation, fire and climate changes over the past one million years. Rev. Micropaléontologie 63, 1–35. https://doi.org/10.1016/j.revmic.2019.02.001, 2019.

Davis, B.A.S., Brewer, S., Stevenson, A.C., Guiot, J.: The temperature of Europe during the Holocene reconstructed from pollen data. Quat. Sci. Rev. 22, 1701–1716. https://doi.org/10.1016/S0277-3791(03)00173-2 , 2003.

Davis, B.A.S., Chevalier, M., Sommer, P., Carter, V.A., Finsinger, W., Mauri, A., Phelps, L.N., Zanon, M., Abegglen, R., Åkesson, C.M., Alba-Sánchez, F., Anderson, R.S., Antipina, T.G., Atanassova, J.R., Beer, R., Belyanina, N.I., Blyakharchuk, T.A., Borisova, O.K., Bozilova, E., Bukreeva, G., Bunting, M.J., Clò, E., Colombaroli, D., Combourieu-Nebout, N., Desprat, S., Di Rita, F., Djamali, M., Edwards, K.J., Fall, P.L., Feurdean, A., Fletcher, W., Florenzano, A., Furlanetto, G., Gaceur, E., Galimov, A.T., Gałka, M., García-Moreiras, I., Giesecke, T., Grindean, R., Guido, M.A., Gvozdeva, I.G., Herzschuh, U., Hjelle, K.L., Ivanov, S., Jahns, S., Jankovska, V., Jiménez-Moreno, G., Karpińska-Kołaczek, M., Kitaba, I., Kołaczek, P., Lapteva, E.G., Latałowa, M., Lebreton, V., Leroy, S., Leydet, M., Lopatina, D.A., López-Sáez, J.A., Lotter, A.F., Magri, D., Marinova, E., Matthias, I., Mavridou, A., Mercuri, A.M., Mesa-Fernández, J.M., Mikishin, Y.A., Milecka, K., Montanari, C., Morales-Molino, C., Mrotzek, A., Muñoz Sobrino, C., Naidina, O.D., Nakagawa, T., Nielsen, A.B., Novenko, E.Y., Panajiotidis, S., Panova, N.K., Papadopoulou, M., Pardoe, H.S., Pędziszewska, A., Petrenko, T.I., Ramos-Román, M.J., Ravazzi, C., Rösch, M., Ryabogina, N., Sabariego Ruiz, S., Salonen, J.S., Sapelko, T.V., Schofield, J.E., Seppä, H., Shumilovskikh, L., Stivrins, N., Stojakowits, P., Svobodova Svitavska, H., Święta-Musznicka, J., Tantau, I., Tinner, W., Tobolski, K., Tonkov, S., Tsakiridou, M., Valsecchi, V., Zanina, O.G., Zimny, M.: The Eurasian Modern Pollen Database (EMPD), Version 2. https://doi.org/10.5194/essd-2020-14, 2020.

Davis, B.A.S., Fasel, M., Kaplan, J.O., Russo, E., Burke, A.: The climate and vegetation of Europe, northern Africa, and the Middle East during the Last Glacial Maximum (21 000 yr BP) based on pollen data. Clim. Past 20, 1939–1988. https://doi.org/10.5194/cp-20-1939-2024, 2024.

De Beaulieu, J.L.: Pollen profile GPILXX, La Grande Pile, France. https://doi.org/10.1594/PANGAEA.739275, 2010.

De Beaulieu, J.-L., Reille, M.: Long Pleistocene pollen sequences from the Velay Plateau (Massif Central, France): I. Ribains maar. Veg. Hist. Archaeobotany 1, 233–242. https://doi.org/10.1007/BF00189500, 1992.

De Beaulieu, J.D., Reille, M.: A long Upper Pleistocene pollen record from Les Echets, near Lyon, France. Boreas 13, 111–132. https://doi.org/10.1111/j.1502-3885.1984.tb00066.x, 1984.

d'Oliveira, L., Dugerdil, L., Ménot, G., Evin, A., Muller, S.D., Ansanay-Alex, S., Azuara, J., Bonnet, C., Bremond, L., Shah, M., Peyron, O.: Reconstructing 15 000 years of southern France temperatures from coupled pollen and molecular (branched glycerol dialkyl glycerol tetraether) markers (Canroute, Massif Central). Clim. Past 19, 2127–2156. https://doi.org/10.5194/cp-19-2127-2023, 2023.

Duprat-Oualid, F., Rius, D., Bégeot, C., Magny, M., Millet, L., Wulf, S., Appelt, O.: Vegetation response to abrupt climate changes in Western Europe from 45 to 14.7k cal a BP: the Bergsee lacustrine record (Black Forest, Germany). J. Quat. Sci. 32, 1008–1021. https://doi.org/10.1002/jqs.2972, 2017.

Dugerdil, L., Ménot, G., Peyron, O., Jouffroy-Bapicot, I., Ansanay-Alex, S., Antheaume, I., Behling, H., Boldgiv, B., Develle, A.-L., Grossi, V., Magail, J., Makou, M., Robles, M., Unkelbach, J., Vannière, B., Joannin, S.: Late Holocene Mongolian climate and environment reconstructions from brGDGTs, NPPs and pollen transfer functions for Lake Ayrag: Paleoclimate implications for Arid Central Asia. Quat. Sci. Rev. 273, 107235, 2021. https://doi.org/10.1016/j.quascirev.2021.107235

Dugerdil, L., Peyron, O., Violle, C., Joannin, S., Ménot, G., Denelle, P., Bruelheide, H., Chytrý, M., Field, R., Hatim, M.Z., Gholizadeh, H., Dolezal, J., Pillar, V.D., Shaltout, K.H., Schrodt, F., Garnier, E.: Functional Signatures of Surface Pollen and Vegetation Are Broadly Similar: Good News for Past Reconstructions of Vegetation. J. Biogeogr. 52, e15100. https://doi.org/10.1111/jbi.15100, 2025.

Dupre Ollivier, M.: Palinologiìa y paleoambiente – nuevos datos españoles referencias, Universidad de Valencia, 160 pp., ISBN 84-7795-000-8, 1988.

Ehlers, J., Giddard, P.L., Hughes, P.D.: Quaternary Glaciations – Extent and Chronology A Closer Look, Elsevier, ISBN 9780444534477. ed., https://doi.org/10.18814/epiiugs/2008/v31i2/004, 2011.

Follieri, M., Magri, D., and Sadori, L.: Pollen stratigraphical synthesis from Valle di Castiglione (Roma), Quaternary Int., 3–4, 81–84, https://doi.org/10.1016/1040-6182(89)90076-1, 1989.

Gebhardt, C., Kühl, N., Hense, A., Litt, T.: Reconstruction of Quaternary temperature fields by dynamically consistent smoothing. Clim. Dyn. 30, 421–437. https://doi.org/10.1007/s00382-007-0299-9, 2008.

Geng, J., Wu, H., Zhang, W., Li, Q., Yu, Y., 2025. Evolution of global vegetation patterns since the last glacial maximum. Quat. Int. 729, 109780. https://doi.org/10.1016/j.quaint.2025.109780

Giardini, M.: Late Quaternary vegetation history at Stracciacappa (Rome, central Italy), Veg. Hist. Archaeobot., 16, 301–316, https://doi.org/10.1007/s00334-006-0037-y, 2007.

Guiot, J., Pons, A., De Beaulieu, J.L., Reille, M.: A 140,000-year continental climate reconstruction from two European pollen records. Nature 338, 309–313. https://doi.org/10.1038/338309a0, 1989.

Guiot, J.: Methodology of the last climatic cycle reconstruction in France from pollen data. Palaeogeogr. Palaeoclimatol. Palaeoecol. 80, 49–69. https://doi.org/10.1016/0031-0182(90)90033-4, 1990.

Guiot, J., Reille, M., De Beaulieu, J.L., Pons, A.: Calibration of the climatic signal in a new pollen sequence from La Grande Pile. Clim. Dyn. 6, 259–264. https://doi.org/10.1007/BF00193539, 1992.

Guiot, J., Torre, F., Jolly, D., Peyron, O., Boreux, J.J., Cheddadi, R.: Inverse vegetation modeling by Monte Carlo sampling to reconstruct palaeoclimates under changed precipitation seasonality and CO2 conditions: application to glacial climate in Mediterranean region. Ecol. Model. 127, 119–140. https://doi.org/10.1016/S0304-3800(99)00219-7, 2000.

Harrison, S.P., Bartlein, P.J., Brewer, S., Prentice, I.C., Boyd, M., Hessler, I., Holmgren, K., Izumi, K., Willis, K.: Climate model benchmarking with glacial and mid-Holocene climates. Clim. Dyn. 43, 671–688. https://doi.org/10.1007/s00382-013-1922-6, 2014.

Harrison, S.P., Prentice, I.C., Barboni, D., Kohfeld, K.E., Ni, J., Sutra, J.-P.: Ecophysiological and bioclimatic foundations for a global plant functional classification. J. Veg. Sci. 21, 300–317. https://doi.org/10.1111/j.1654-1103.2009.01144.x, 2010.

Haywood, A.M., Dowsett, H.J., Valdes, P.J., Lunt, D.J., Francis, J.E., Sellwood, B.W.: Introduction. Pliocene climate, processes and problems. Philos. Trans. R. Soc. Math. Phys. Eng. Sci. 367, 3–17. https://doi.org/10.1098/rsta.2008.0205, 2009.

Hengl, T., Walsh, M.G., Sanderman, J., Wheeler, I., Harrison, S.P., Prentice, I.C.: Global mapping of potential natural vegetation: an assessment of machine learning algorithms for estimating land potential. PeerJ 6, e5457. https://doi.org/10.7717/peerj.5457, 2018.

Hersbach, H., Bell, B., Berrisford, P., Hirahara, S., Horányi, A., Muñoz-Sabater, J., Nicolas, J., Peubey, C., Radu, R., Schepers, D., Simmons, A., Soci, C., Abdalla, S., Abellan, X., Balsamo, G., Bechtold, P., Biavati, G., Bidlot, J., Bonavita, M., De Chiara, G., Dahlgren, P., Dee, D., Diamantakis, M., Dragani, R., Flemming, J., Forbes, R., Fuentes, M., Geer, A., Haimberger, L., Healy, S., Hogan, R.J., Hólm, E., Janisková, M., Keeley, S., Laloyaux, P., Lopez, P., Lupu, C., Radnoti, G., De Rosnay, P., Rozum, I., Vamborg, F., Villaume, S., Thépaut, J.: The ERA5 global reanalysis. Q. J. R. Meteorol. Soc. 146, 1999–2049. https://doi.org/10.1002/qj.3803, 2020.

Herzschuh, U., Böhmer, T., Chevalier, M., Dallmeyer, A., Li, C., Cao, X., Hébert, R., Peyron, O., Nazarova, L., Novenko, E.Y., Park, J., Rudaya, N.A., Schlütz, F., Shumilovskikh, L.S., Tarasov, P.E., Wang, Y., Wen, R., Xu, Q., Zheng, Z.: Regional pollen-based Holocene temperature and precipitation patterns depart from the Northern Hemisphere mean trends. https://doi.org/10.5194/egusphere-2022-127, 2022a.

Herzschuh, U., Böhmer, T., Li, C., Chevalier, M., Hébert, R., Cao, X., Bigelow, N.H., Nazarova, L., Novenko, E.Y., Peyron, O., Rudaya, N.A., Schlütz, F., Shumilovskikh, L.S.: 1 LegacyClimate 1.0: A dataset of pollen-based climate 2 reconstructions from 2594 Northern Hemisphere sites covering the 3 last 30 ka and beyond., Earth Syst. Sci. Data, 15, 2235–2258, https://doi.org/10.5194/essd-15-2235-2023, 2022b.

Hughes, P.D., Gibbard, P.L., Ehlers, J.: Timing of glaciation during the last glacial cycle: evaluating the concept of a global 'Last Glacial Maximum' (LGM). Earth-Sci. Rev. 125, 171–198. https://doi.org/10.1016/j.earscirev.2013.07.003, 2013.

Izumi, K., Bartlein, P.J., Harrison, S.P.: Consistent large-scale temperature responses in warm and cold climates. Geophys. Res. Lett. 40, 1817–1823. https://doi.org/10.1002/grl.50350, 2013.

Jalut, G., Marti, J. M., Fontugne, M., Delibrias, G., Vilaplana, J. M., and Julia, R.: Glacial to interglacial vegetation changes in the northern and southern Pyrénées: Deglaciation, vegetation cover and chronology, Quaternary Sci. Rev., 11, 449–480, https://doi.org/10.1016/0277-3791(92)90027-6, 1992.

Jost, A., Lunt, D., Kageyama, M., Abe-Ouchi, A., Peyron, O., Valdes, P.J., Ramstein, G.: High-resolution simulations of the last glacial maximum climate over Europe: a solution to discrepancies with continental palaeoclimatic reconstructions? Clim. Dyn. 24, 577–590. https://doi.org/10.1007/s00382-005-0009-4, 2005.

Juggins, S.: Quantitative reconstructions in palaeolimnology: new paradigm or sick science? Quat. Sci. Rev. 64, 20–32. https://doi.org/10.1016/j.quascirev.2012.12.014, 2013.

Joussaume, S., Taylor, K.E., Braconnot, P., Mitchell, J.F.B., Kutzbach, J.E., Harrison, S.P., Prentice, I.C., Broccoli, A.J., Abe-Ouchi, A., Bartlein, P.J., Bonfils, C., Dong, B., Guiot, J., Herterich, K., Hewitt, C.D., Jolly, D., Kim, J.W., Kislov, A., Kitoh, A., Loutre, M.F., Masson, V., McAvaney, B., McFarlane, N., De Noblet, N., Peltier, W.R., Peterschmitt, J.Y., Pollard, D., Rind, D., Royer, J.F., Schlesinger, M.E., Syktus, J., Thompson, S., Valdes, P., Vettoretti, G., Webb, R.S., Wyputta, U.: Monsoon changes for 6000 years ago: Results of 18 simulations from the Paleoclimate Modeling Intercomparison Project (PMIP). Geophys. Res. Lett. 26, 859–862. https://doi.org/10.1029/1999GL900126, 1999.

Juggins, S.: Rioja: Analysis of Quaternary Science Data. https://doi.org/https: //cran.r-project.org/package=rioja, http://www.staff.ncl.ac.uk/stephen.juggins/, 2020.

Kageyama, M., Harrison, S.P., Kapsch, M.-L., Lofverstrom, M., Lora, J.M., Mikolajewicz, U., Sherriff-Tadano, S., Vadsaria, T., Abe-Ouchi, A., Bouttes, N., Chandan, D., Gregoire, L.J., Ivanovic, R.F., Izumi, K., LeGrande, A.N., Lhardy, F., Lohmann, G., Morozova, P.A., Ohgaito, R., Paul, A., Peltier, W.R., Poulsen, C.J., Quiquet, A., Roche, D.M., Shi, X., Tierney, J.E., Valdes, P.J., Volodin, E., Zhu, J.: The PMIP4 Last Glacial Maximum experiments: preliminary results and comparison with the PMIP3 simulations. Clim. Past 17, 1065–1089. https://doi.org/10.5194/cp-17-1065-2021, 2021.

Kaplan, J.O., Pfeiffer, M., Kolen, J.C.A., Davis, B.A.S.: Large Scale Anthropogenic Reduction of Forest Cover in Last Glacial Maximum Europe. PLOS ONE 11, e0166726. https://doi.org/10.1371/journal.pone.0166726, 2016.

Kaplan, J.O., Bigelow, N.H., Prentice, I.C., Harrison, S.P., Bartlein, P.J., Christensen, T.R., Cramer, W., Matveyeva, N.V., McGuire, A.D., Murray, D.F., Razzhivin, V.Y., Smith, B., Walker, D.A., Anderson, P.M., Andreev, A.A., Brubaker, L.B., Edwards, M.E., Lozhkin, A.V.: Climate change and Arctic ecosystems: 2. Modeling, paleodata-model comparisons, and future projections. J. Geophys. Res. Atmospheres 108, 2002JD002559. https://doi.org/10.1029/2002JD002559, 2003.

Kern, O.A., Maier, A., Vercauteren, N.: Landscape reconstructions for Europe during the late Last Glacial (60–20 ka BP): A pollen-based REVEALS approach. https://doi.org/10.5194/essd-2024-306, 2024.

Kern, O.A., Koutsodendris, A., Pross, J.: Palynological data for the Late Glacial and Holocene (14.5–0 ka BP) from Füramoos, Southern Germany. Data Brief 39, 107650. https://doi.org/10.1016/j.dib.2021.107650, 2021.

Kühl, N., Gebhardt, C., Litt, T., Hense, A.: Probability Density Functions as Botanical-Climatological Transfer Functions for Climate Reconstruction. Quat. Res. 58, 381–392. https://doi.org/10.1006/qres.2002.2380, 2002.

Kühl, N., Moschen, R., Wagner, S., Brewer, S., Peyron, O.: A multiproxy record of late Holocene natural and anthropogenic environmental change from the Sphagnum peat bog Dürres Maar, Germany: implications for quantitative climate reconstructions based on pollen. J. Quat. Sci. 25, 675–688. https://doi.org/10.1002/jqs.1342, 2010.

Kühl, N., Litt, T.: Quantitative time series reconstruction of Eemian temperature at three European sites using pollen data. Veg. Hist. Archaeobotany 12, 205–214. https://doi.org/10.1007/s00334-003-0019-2, 2003.

Küster, H.: Postglaziale Vegetationsgeschichte Südbayerns, Geobotanische Studien zur Prähistorischen Landschaftskunde, Akademie Verlag, Berlin, ISBN 978-3-05-501592-2, 1995.

Li, C., Dallmeyer, A., Ni, J., Chevalier, M., Willeit, M., Andreev, A.A., Cao, X., Schild, L., Heim, B., Herzschuh, U.: Global biome changes over the last 21,000 years inferred from model-data comparisons. https://doi.org/10.5194/egusphere-2024-1862, 2024.

Liu, M., Prentice, I.C., Ter Braak, C.J.F., Harrison, S.P.: An improved statistical approach for reconstructing past climates from biotic assemblages. Proc. R. Soc. Math. Phys. Eng. Sci. 476, 20200346. https://doi.org/10.1098/rspa.2020.0346, 2020.

Valero-Garcés, B. L., González-Sampériz, P., Navas, A., Machin, J., Delgado-Huertas, A., Pena-Monné, J. L., Sancho-Marcén, C., Stevenson, T., and Davis, B.: Paleohydrological fluctuations and steppe vegetation during the last glacial maximum in the central Ebro valley (NE Spain), Quatern. Int., 122, 43–55, https://doi.org/10.1016/j.quaint.2004.01.030, 2004.

Magyari, E. K., Pál, I., Vincze, I., Veres, D., Jakab, G., Braun, M., Szalai, Z., Szabó, Z., and Korponai, J.: Warm Younger Dryas summers and early late glacial spread of temperate deciduous trees in the Pannonian Basin during the last glacial termination (20–9 kyr cal BP), Quat. Sci. Rev., 225, 105980, https://doi.org/10.1016/j.quascirev.2019.105980, 2019.

Magyari, E. K., Kuneš, P., Jakab, G., Sümegi, P., Pelánková, B., Schäbitz, F., Braun, M., and Chytrý, M.: Late Pleniglacial vegetation in eastern-central Europe: Are there modern analogues in Siberia?, Quaternary Sci. Rev., 95, 60–79, https://doi.org/10.1016/j.quascirev.2014.04.020, 2014.

Magyari, E., Jakab, G., Rudner, E., and Sümegi, P.: Palynological and plant macrofossil data on Late Pleistocene short-term climatic oscillations in NE-Hungary, Acta Palaeobot. Suppl., 2, 491–502, 1999.

Magri, D. and Sadori, L.: Late Pleistocene and Holocene pollen stratigraphy at Lago di Vico, central Italy, Veg. Hist. Archaeobot., 8, 247–260, https://doi.org/10.1007/BF01291777, 1979.

Margari, V., Gibbard, P. L., Bryant, C. L., and Tzedakis, P. C.: Character of vegetational and environmental changes in southern Europe during the last glacial period; evidence from Lesvos Island, Greece, Quaternary Sci. Rev., 28, 1317–1339, https://doi.org/10.1016/j.quascirev.2009.01.008, 2009.

Marinova, E., Harrison, S. P., Bragg, F., Connor, S., de Laet, V., Leroy, S. A. G., Mudie, P., Atanassova, J., Bozilova, E., Caner, H., Cordova, C., Djamali, M., Filipova-Marinova, M., Gerasimenko, N., Jahns, S., Kouli, K., Kotthoff, U., Kvavadze, E., Lazarova, M., Novenko, E., Ramezani, E., Röpke, A., Shumilovskikh, L., Tanţău, I., and Tonkov, S.: Pollen-derived biomes in the Eastern Mediterranean–Black Sea–Caspian-Corridor, J. Biogeogr., 45, 484–499, https://doi.org/10.1111/jbi.13128, 2019.

Martin, C., Ménot, G., Thouveny, N., Peyron, O., Andrieu-Ponel, V., Montade, V., Davtian, N., Reille, M., Bard, E.: Early Holocene Thermal Maximum recorded by branched tetraethers and pollen in Western Europe (Massif Central, France). Quat. Sci. Rev. 228, 106109. https://doi.org/10.1016/j.quascirev.2019.106109, 2020.

Mauri, A., Davis, B.A.S., Collins, P.M., Kaplan, J.O.: The climate of Europe during the Holocene: a gridded pollen-based reconstruction and its multi-proxy evaluation. Quat. Sci. Rev. 112, 109–127. https://doi.org/10.1016/j.quascirev.2015.01.013, 2015.

Mauri, A., Davis, B.A.S., Collins, P.M., Kaplan, J.O.: The influence of atmospheric circulation on the mid-Holocene climate of Europe: a data–model comparison. Clim. Past 10, 1925–1938. https://doi.org/10.5194/cp-10-1925-2014, 2014.

Miebach, A., Niestrath, P., Roeser, P., and Litt, T.: Impacts of climate and humans on the vegetation in northwestern Turkey: palynological insights from Lake Iznik since the Last Glacial, Clim. Past, 12, 575–593, https://doi.org/10.5194/cp-12575-2016, 2016.

Miola, A., Bondesan, A., Corain, L., Favaretto, S., Mozzi, P., Piovan, S., and Sostizzo, I.: Wetlands in the Venetian Po Plain (northeastern Italy) during the Last Glacial Maximum: Interplay between vegetation, hydrology and sedimentary environment, Rev. Palaeobot. Palynol., 141, 53–81, https://doi.org/10.1016/j.revpalbo.2006.03.016, 2006.

Monegato, G., Ravazzi, C., Donegana, M., Pini, R., Calderoni, G., and Wick, L.: Evidence of a two-fold glacial advance during the last glacial maximum in the Tagliamento end moraine system (eastern Alps), Quatern. Res., 68, 284–302, https://doi.org/10.1016/j.yqres.2007.07.002, 2007.

Netzel, T., Miebach, A., Litt, T., Hense, A.: New probabilistic methods for quantitative climate reconstructions applied to palynological data from Lake Kinneret. Clim. Past 21, 357–380. https://doi.org/10.5194/cp-21-357-2025, 2025.

Ortega-Rosas, C.I., Guiot, J., Peñalba, M.C., Ortiz-Acosta, M.E.: biomisation and quantitative climate reconstruction techniques in northwestern Mexico—With an application to four Holocene pollen sequences. Glob. Planet. Change 61, 242–266. https://doi.org/10.1016/j.gloplacha.2007.10.006, 2008.

Overpeck, J.T., Webb, T., Prentice, I.C.: Quantitative Interpretation of Fossil Pollen Spectra: Dissimilarity Coefficients and the Method of Modern Analogs. Quat. Res. 23, 87–108. https://doi.org/10.1016/0033-5894(85)90074-2, 1985.

Paganelli, A.: Evolution of vegetation and climate in the Veneto-Po Plain during the Late-Glacial and Early Holocene using pollenstrat-igraphical data, Alp. Mediterr. Quat., 9, 581–589, 1996.

Peltier, W.R., Solheim, L.P.: The climate of the Earth at Last Glacial Maximum: statistical equilibrium state and a mode of internal variability. Quat. Sci. Rev. 23, 335–357. https://doi.org/10.1016/j.quascirev.2003.07.003, 2004.

Pérez-Obiol, R. P. and Julia, R.: Climatic change on the Iberian Peninsula recorded in a 30,000-year pollen record from Lake Banyoles, Quaternary Res., 41, 91–98, 1994.

Peyron, O., Magny, M., Goring, S., Joannin, S., De Beaulieu, J.-L., Brugiapaglia, E., Sadori, L., Garfi, G., Kouli, K., Ioakim, C., Combourieu-Nebout, N.: Contrasting patterns of climatic changes during the Holocene across the Italian Peninsula reconstructed from pollen data. Clim. Past 9, 1233–1252. https://doi.org/10.5194/cp-9-1233-2013, 2013.

Peyron, O., Bégeot, C., Brewer, S., Heiri, O., Magny, M., Millet, L., Ruffaldi, P., Van Campo, E., Yu, G.: Late-Glacial climatic changes in Eastern France (Lake Lautrey) from pollen, lake-levels, and chironomids. Quat. Res. 64, 197–211. https://doi.org/10.1016/j.yqres.2005.01.006, 2005.

Peyron, O., Guiot, J., Cheddadi, R., Tarasov, P., Reille, M., De Beaulieu, J.-L., Bottema, S., Andrieu, V.: Climatic Reconstruction in Europe for 18,000 YR B.P. from

Pollen Data. Quat. Res. 49, 183–196. https://doi.org/10.1006/qres.1997.1961, 1998.

Pini, R., Ravazzi, C., and Donegana, D.: Pollen stratigraphy, vegetation and climate history of the last 215 ka in the Azzano Decimo core (plain of Friuli, north-eastern Italy), Quaternary Sci. Rev., 28, 1268–1290, https://doi.org/10.1016/j.quascirev.2008.12.017, 2009.

Prentice, I.C., Villegas-Diaz, R., Harrison, S.P.: Accounting for atmospheric carbon dioxide variations in pollen-based reconstruction of past hydroclimates. Glob. Planet. Change 211, 103790. https://doi.org/10.1016/j.gloplacha.2022.103790, 2022.

Prentice, I.C., Harrison, S.P., Jolly, D.: The climate and biomes of europe at 6000 yr bp: comparison of model simulations and pollen-based reconstructions. Quaternary Science Reviews, 1998, 17 (6-7), pp.659-668. https://doi.org/10.1016/S0277-3791(98)00016-X, 1998.

Prentice, I.C., Webb Iii, T.: BIOME 6000: reconstructing global mid-Holocene vegetation patterns from palaeoecological records. J. Biogeogr. 25, 997–1005. https://doi.org/10.1046/j.1365-2699.1998.00235.x, 1998.

Prentice, I.C., Guiot, J., Huntley, B., Jolly, D., Cheddadi, R.: Reconstructing biomes from palaeoecological data: a general method and its application to European pollen data at 0 and 6 ka. Clim. Dyn. 12, 185–194, 1996.

Prentice, I.C., Cramer, W., Harrison, S.P., Leemans, R., Monserud, R.A., Solomon, A.M.: Special Paper: A Global Biome Model Based on Plant Physiology and Dominance, Soil Properties and Climate. J. Biogeogr. 19, 117. https://doi.org/10.2307/2845499, 1992.

Ramstein, G., Kageyama, M., Guiot, J., Wu, H., Hély, C., Krinner, G., and Brewer, S.: How cold was Europe at the Last Glacial Maximum? A synthesis of the progress achieved since the first PMIP model-data comparison, Clim. Past, 3, 331–339, https://doi.org/10.5194/cp-3-331-2007, 2007.

Reille, M. and Andrieu, V.: The late Pleistocene and Holocene in the Lourdes Basin, Western Pyrénées, France: new pollen analytical and chronological data, Veg. Hist. Archaeobot., 4, 1–21, https://doi.org/10.1007/BF00198611, 1995.

Reimer, P.J., Austin, W.E.N., Bard, E., Bayliss, A., Blackwell, P.G., Bronk Ramsey, C., Butzin, M., Cheng, H., Edwards, R.L., Friedrich, M., Grootes, P.M., Guilderson, T.P., Hajdas, I., Heaton, T.J., Hogg, A.G., Hughen, K.A., Kromer, B., Manning, S.W., Muscheler, R., Palmer, J.G., Pearson, C., Van Der Plicht, J., Reimer, R.W., Richards, D.A., Scott, E.M., Southon, J.R., Turney, C.S.M., Wacker, L., Adolphi, F., Büntgen, U., Capano, M., Fahrni, S.M., Fogtmann-Schulz, A., Friedrich, R., Köhler, P., Kudsk, S., Miyake, F., Olsen, J., Reinig, F., Sakamoto, M., Sookdeo, A., Talamo, S.: The IntCal20 Northern Hemisphere Radiocarbon Age Calibration Curve (0–55 cal kBP). Radiocarbon 62, 725–757. https://doi.org/10.1017/RDC.2020.41, 2020.

Robles, M., Peyron, O., Ménot, G., Brugiapaglia, E., Wulf, S., Appelt, O., Blache, M., Vannière, B., Dugerdil, L., Paura, B., Ansanay-Alex, S., Cromartie, A., Charlet, L., Guédron, S., De Beaulieu, J.-L., Joannin, S.: Climate changes during the Late Glacial in southern Europe: new insights based on pollen and brGDGTs of Lake Matese in Italy. Clim. Past 19, 493–515. https://doi.org/10.5194/cp-19-493-2023, 2023.

Sadori, L., Koutsodendris, A., Panagiotopoulos, K., Masi, A., Bertini, A., Combourieu-Nebout, N., Francke, A., Kouli, K., Joannin, S., Mercuri, A.M., Peyron, O., Torri, P., Wagner, B., Zanchetta, G., Sinopoli, G., Donders, T.H.: Pollen-based paleoenvironmental and paleoclimatic change at Lake Ohrid (south-eastern Europe) during the past 500 ka. Biogeosciences 13, 1423–1437. https://doi.org/10.5194/bg-13-1423-2016, 2016.

Salonen, J.S., Korpela, M., Williams, J.W., Luoto, M.: Machine-learning based reconstructions of primary and secondary climate variables from North American and European fossil pollen data. Sci. Rep. 9, 15805. https://doi.org/10.1038/s41598-019-52293-4, 2019.

Sánchez Goñi, M.F., Desprat, S., Daniau, A.-L., Bassinot, F.C., Polanco-Martínez, J.M., Harrison, S.P., Allen, J.R.M., Anderson, R.S., Behling, H., Bonnefille, R., Burjachs, F., Carrión, J.S., Cheddadi, R., Clark, J.S., Combourieu-Nebout, N., Mustaphi, Colin.J.C., Debusk, G.H., Dupont, L.M., Finch, J.M., Fletcher, W.J., Giardini, M., González, C., Gosling, W.D., Grigg, L.D., Grimm, E.C., Hayashi, R., Helmens, K., Heusser, L.E., Hill, T., Hope, G., Huntley, B., Igarashi, Y., Irino, T., Jacobs, B., Jiménez-Moreno, G., Kawai, S., Kershaw, A.P., Kumon, F., Lawson, I.T., Ledru, M.-P., Lézine, A.-M., Liew, P.M., Magri, D., Marchant, R., Margari, V., Mayle, F.E., McKenzie, G.M., Moss, P., Müller, S., Müller, U.C., Naughton, F., Newnham, R.M., Oba, T., Pérez-Obiol, R., Pini, R., Ravazzi, C., Roucoux, K.H., Rucina, S.M., Scott, L., Takahara, H., Tzedakis, P.C., Urrego, D.H., Van Geel, B., Valencia, B.G., Vandergoes, M.J., Vincens, A., Whitlock, C.L., Willard, D.A., Yamamoto, M.: The ACER pollen and charcoal database: a global resource to document vegetation and fire response to abrupt climate changes during the last glacial period. Earth Syst. Sci. Data 9, 679–695. https://doi.org/10.5194/essd-9-679-2017, 2017.

Sassoon, D., Combourieu-Nebout, N., Peyron, O., Bertini, A., Toti, F., Lebreton, V., Moncel, M.-H.: Pollen-based climatic reconstructions for the interglacial analogues of MIS 1 (MIS 19, 11, and 5) in the southwestern Mediterranean: insights from ODP Site 976. Clim. Past 21, 489–515. https://doi.org/10.5194/cp-21-489-2025, 2025.

Satkunas, J. and Grigiene , A.: Eemian-Weichselian palaeoenvironmental record from the Micku nai glacial depression (Eastern Lithuania), Geologija, 54, 35–51, https://doi.org/10.6001/geologija.v54i2.2482, 2012.

Seguinot, J., Ivy-Ochs, S., Jouvet, G., Huss, M., Funk, M., Preusser, F.: Modelling last glacial cycle ice dynamics in the Alps. The Cryosphere 12, 3265–3285. https://doi.org/10.5194/tc-12-3265-2018, 2018.

Šeirienė, V., Kühl, N., Kisielienė, D.: Quantitative reconstruction of climate variability during the Eemian (Merkinė) and Weichselian (Nemunas) in Lithuania. Quat. Res. 82, 229–235. https://doi.org/10.1016/j.yqres.2014.04.004, 2014.

Seltzer, A.M., Blard, P.-H., Sherwood, S.C., Kageyama, M.: Terrestrial amplification of past, present, and future climate change. Sci. Adv. 9, eadf8119. https://doi.org/10.1126/sciadv.adf8119, 2023.

Sinopoli, G., Masi, A., Regattieri, E., Wagner, B., Francke, A., Peyron, O., Sadori, L.: Palynology of the Last Interglacial Complex at Lake Ohrid: palaeoenvironmental and palaeoclimatic inferences. Quat. Sci. Rev. 180, 177–192. https://doi.org/10.1016/j.quascirev.2017.11.013, 2018.

Sirocko, Frank; Knapp, Hannes; Dreher, Frank; Förster, Michael W; Albert, Johannes; Brunck, Heiko; Veres, Daniel; Dietrich, Stephan; Zech, Michael; Hambach, Ulrich; Röhner, Marieke; Rudert, Saskia; Schwiebus, Klaus; Adams, Christel; Sigl, Petra.: The ELSA-Vegetation-Stack: Reconstruction of Landscape Evolution Zones (LEZ) from laminated Eifel maar sediments of the last 60,000 years. Global and Planetary Change, 142, 108-135, https://doi.org/10.1016/j.gloplacha.2016.03.005, 2016.

Strahl, J.: Zur Pollenstratigraphie des Weichselspätglazials von Berlin-Brandenburg [On the palynostratigraphy of the Late Weichselian in Berlin-Brandenburg], Brand. Geowissensch. Beitr., 12, 87–112, 2005.

Tarasov, P.E., Müller, S., Zech, M., Andreeva, D., Diekmann, B., Leipe, C.: Last glacial vegetation reconstructions in the extreme-continental eastern Asia: Potentials of pollen and n-alkane biomarker analyses. Quat. Int. 290–291, 253–263. https://doi.org/10.1016/j.quaint.2012.04.007, 2013.

Tarasov, P.E., Peyron, O., Guiot, J., Brewer, S., Volkova, V.S., Bezusko, L.G., Dorofeyuk, N.I., Kvavadze, E.V., Osipova, I.M., Panova, N.K.: Last Glacial Maximum climate of the former Soviet Union and Mongolia reconstructed from pollen and plant macrofossil data. Clim. Dyn. 15, 227–240. https://doi.org/10.1007/s003820050278, 1999.

Tarasov, P.E., Volkova, V.S., Iii, T.W., Guiot, J., Andreev, A.A., Bezusko, L.G., Bykova, G.V., Dorofeyuk, N.I., Kvavadze, E.V., Osipova, I.M., Panova, N.K., Sevastyanov, D.V.: Black well Science, Ltd Last glacial maximum biomes reconstructed from pollen and plant macrofossil data from northern Eurasia. J. Biogeogr., 27, 609-620, https://doi.org/10.1046/j.1365-2699.2000.00429.x, 2000.

Ter Braak, C.J.F., Juggins, S.: Weighted averaging partial least squares regression (WA-PLS): an improved method for reconstructing environmental variables from species assemblages. Hydrobiologia 485–502, 1993.

Tonkov, S., Lazarova, M., Bozilova, E., Ivanov, D., Snowball.I.: A 30,000-year pollen record from Mire Kupena, Western Rhodopes Mountains (south Bulgaria). Rev. Palaeobot. Palynol. 209, 41–51. https://doi.org/10.1016/j.revpalbo.2014.06.002, 2014.

Trasune, L., Väliranta, M., Stivrins, N., Amon, L., Schenk, F., Salonen, J.S.: A comparison of plant macrofossil-based quantitative climate reconstruction methods: A case study of the lateglacial Baltic States. Quat. Sci. Rev. 338, 108811. https://doi.org/10.1016/j.quascirev.2024.108811, 2024.

Tzedakis, P. C., Frogley, M. R., Lawson, I. T., Preece, R. C., Cacho, I., and de Abreu, L.: Ecological thresholds and patterns of millennial-scale climate variability: The response of vegetation in Greece during the last glacial period, Geology, 32, 109–112, https://doi.org/10.1130/G20118.1, 2004.

Vegas-Vilarrúbia, T., González-Sampériz, P., Morellón, M., GilRomera, G., Pérez-Sanz, A., and Valero-Garcés, B.: Diatom and vegetation responses to late glacial and early holocene climate changes at lake estanya (southern pyrenees, NE spain), Palaeogeogr. Palaeoclim. Palaeoecol., 392, 335–349, https://doi.org/10.1016/j.palaeo.2013.09.011, 2013.

Viau, A.E., Gajewski, K.: Reconstructing Millennial-Scale, Regional Paleoclimates of Boreal Canada during the Holocene. J. Clim. 22, 316–330. https://doi.org/10.1175/2008JCLI2342.1, 2009.

Watts, W. A., Allen, J. R. M., and Huntley, B.: Vegetation history and palaeoclimate of the last glacial period at Lago grande di Monticchio, southern Italy, Quaternary Sci. Rev., 15, 133–153, https://doi.org/10.1016/0277-3791(95)00093-3, 1996.

Williams, J.W., Shuman, B.: Obtaining accurate and precise environmental reconstructions from the modern analog technique and North American surface pollen dataset. Quat. Sci. Rev. 27, 669–687. https://doi.org/10.1016/j.quascirev.2008.01.004, 2008

Wu, H., Guiot, J., Brewer, S., Guo, Z.: Climatic changes in Eurasia and Africa at the last glacial maximum and mid-Holocene: reconstruction from pollen data using inverse vegetation modelling. Clim. Dyn. 29, 211–229. https://doi.org/10.1007/s00382-007-0231-3, 2007.

Xu, Q., Zhang, S., Gaillard, M., Li, M., Cao, X., Tian, F., Li, F.: Studies of modern pollen assemblages for pollen dispersal- deposition- preservation process understanding and for pollen-based reconstructions of past vegetation, climate, and human impact: A review based on case studies in China. Quat. Sci. Rev. 149, 151–166. https://doi.org/10.1016/j.quascirev.2016.07.017, 2016.